

Prospects of Indirect Detection for the Heavy S3 Dark Doublet

C. Espinoza^{*1} and M. Mondragón^{†2}

¹*Cátedras Conacyt - Instituto de Física, Universidad Nacional Autónoma de México, Apdo. Postal 20-364, Cd. México 01000, México.*

²*Instituto de Física, Universidad Nacional Autónoma de México, Apdo. Postal 20-364, Cd. México 01000, México.*

Abstract

We present an analysis of the Dark S3 model in the heavy DM mass region, this model features an S3 symmetric extension of the scalar sector of the SM including a scalar $SU(2)$ doublet dark matter candidate. We use publicly available tools to compute, in addition to conventional physical constraints on the parameter space of the model, the Sommerfeld enhancement factors for the present day annihilation cross section and the likelihood profile for a simulation of an observation run by the Cherenkov Telescope Array of the Coma Berenices dwarf galaxy. Our results disfavour masses above ~ 5 TeV mainly because of overproduction of dark matter not consistent with the relic abundance observations; we also find a moderately large region with masses in between 1.2 and 4.9 TeV which predict the correct value of the DM relic and in addition have a light scalar with the characteristics of the SM Higgs boson (i.e. within the decoupling limit akin to the THDM). Comparison of our results with model independent exclusion curves from HESS and other CTA simulations show that these limits fall short only an order of magnitude in the value of the annihilation cross section in order to exclude the best fit point of the model.

1 Introduction

The study of extensions of the Standard Model (SM) capable of tackling one or more of the well known issues present in this paradigm of particle physics continues to be one of the most active fields of contemporary research. One strategy is to approach the subject from the scalar sector of the SM, enlarging its field content with extra scalars while keeping the rest of the sectors untouched. As demonstrated by the vast literature on the Two Higgs Doublet Model (THDM), the simplest of such extensions, the possibility of stumbling into rich and interesting phenomenology is just around the corner (see e.g. [1] and references therein). Moreover, by taking the extra scalar doublet as inert (the Inert Doublet Model (IDM) [2]) we end up with a very simple and at the same time highly illustrative model containing a candidate for dark matter with rich phenomenology, e.g. see for example [3–37].

^{*}m.catalina@fisica.unam.mx

[†]myriam@fisica.unam.mx

Multihiggs models are natural generalizations of this scheme, including those with additional symmetries imposed, for example the $S3$ symmetric model where a total of three Higgs doublets are present and it is assumed that these scalars (and the matter sector) belong to irreducible representations of the permutation group $S3$ reflecting a hypothesized discrete symmetry of the model, motivated in part by the fact that matter particles of a given flavor are only distinguishable from other flavors by their masses and therefore are identical to each other before electroweak symmetry breaking (EWSB). The study of these models was pioneered in [38–40] which has led to subsequent interesting research, see e.g. [41–59].

In this letter we continue our research initiated in [53] wherein we exploit the fact that the permutation group $S3$ has four irreducible representations, this leaves just enough space to augment to the $S3$ symmetric model a fourth scalar doublet which, when taken as inert, comprises a simple IDM-like dark sector. This time, we focus our attention on the high (1 – 20 TeV) DM candidate mass region of the parameter space of the model exploring the possibilities of indirect detection (ID) of gamma ray signals specifically in the Cherenkov Telescope Array (CTA), from a simulated observation of the dwarf spheroidal galaxy Coma Berenices¹. In this large mass regime it is important to take into account the nonperturbative phenomenon of Sommerfeld enhancement which is a manifestation of the multiple exchanges of gauge bosons and higgses between two annihilating DM particles, specially for the correct analysis of the gamma ray fluxes predicted by the model whose detection is the holy grail of dark matter ID experiments. This phenomenon occurs because the DM particles move at present with nonrelativistic (NR) velocities ($\sim 10^{-3}$) and (colloquially speaking) they have enough time to exchange (on-shell) mediators before the actual annihilation. As a result, the wave function of the DM pair is no longer a plane wave and to correctly predict the annihilation cross section it is necessary to find out the modified wave function. This process becomes particular important when the mass of the DM candidate is much larger than the gauge bosons and higgses because then the electroweak force between the DM pair becomes “long range”, and also when there are other particles in the dark sector such as those part of the same multiplet of $SU(2)$ as the DM candidate, because then the EWSB induced mass splitting between these particles is relatively small and as a result the exchange of mediators can induce transitions of the original annihilating DM pair to other states in the multiplet, which potentially enhances the annihilation cross section.

Thus, for our analysis we compute the predicted DM annihilating gamma ray flux with Sommerfeld corrections from the mentioned dwarf galaxy and use this prediction to obtain a likelihood estimate from a simulated observation at the CTA. Specifically, we simulate a null-result experiment, meaning that we assume that during the observation period no significant gamma ray signal above background was encountered, this permits us to obtain a likelihood estimate and a test statistics (TS) from the comparison of both hypothesis, the existence or non-existence of a signal from DM annihilation, which in turn leads to the estimate of limiting or exclusion regions for the parameter space of the model. In order to obtain such information of the parameter space we perform a directed scan, for each probed point (set of values of the independent parameters) in the model we feed the predicted flux to the public CTA analysis tools obtaining a likelihood estimate and a TS, we then supplement the estimated likelihood with information regarding unitarity and collider constraints on heavy scalars as well as the comparison with the relic abundance experimental value. For simplicity, we neither reject points on account of violating unitarity or collider bounds nor define additional likelihood functions to deal with these constraints. Instead, equivalently, we simply penalize the CTA likelihood estimate when this happens as well as when the predicted relic

¹ As explain in section 4 due to the large dimensionality of the parameter space the work load of the calculation of the likelihood profile makes analyzing more than one dwarf rather unfeasible with the computational resources at our disposal.

abundance is above the experimental value, but we allow for points with relic abundance predictions below this bound to account for the possibility of under-abundant DM component. Our analysis allows us to present a likelihood profile of the parameter space of the model and estimate to what extent future observations of the CTA array can probe the model.

2 Flux from annihilating DM pairs

2.1 The model

The $S3$ -model is an extension of the scalar sector of the SM with a total of three $SU(2)$ doublets which, together with the matter sector, are assumed to transform under the permutation group $S3$ in such a manner that the Lagrangian respects the symmetry even after EWSB. Two of the EW doublets, Φ_1 and Φ_2 are chosen to form an $S3$ doublet while the third one Φ_s transforms as a symmetric singlet of $S3$; the matter sector is chosen to have transformation properties as in reference [47]. We take advantage of the fact that the $S3$ group has four irreducible representations which allows us to introduce a dark sector in the model by including an extra $SU(2)$ doublet, Φ_a , transforming as an antisymmetric singlet of $S3$ and imposing a Z_2 discrete symmetry under which the only field with nontrivial transformation is Φ_a . The dark sector scalar potential is constructed as follows:

$$V_{\text{DM}} = V_{2a} + V_{4a} + V_{4sa} \quad (1)$$

where each term is given respectively by:

$$V_{2a} = \mu_2^2 \Phi_a^\dagger \Phi_a \quad (2)$$

$$\begin{aligned} V_{4a} = & \lambda_{10}(\Phi_a^\dagger \Phi_a)(\Phi_1^\dagger \Phi_1 + \Phi_2^\dagger \Phi_2) \\ & + \lambda_{11}[(\Phi_a^\dagger \Phi_1)(\Phi_1^\dagger \Phi_a) + (\Phi_a^\dagger \Phi_2)(\Phi_2^\dagger \Phi_a)] \\ & + \lambda_{12}[(\Phi_a^\dagger \Phi_1)(\Phi_a^\dagger \Phi_1) + (\Phi_a^\dagger \Phi_2)(\Phi_a^\dagger \Phi_2) + \text{h.c.}] \\ & + \lambda_{13}(\Phi_a^\dagger \Phi_a)^2 \end{aligned} \quad (3)$$

$$V_{4sa} = \lambda_{14}(\Phi_s^\dagger \Phi_a \Phi_a^\dagger \Phi_s) \quad (4)$$

For the full Lagrangian and complete details of the model we refer the reader to our previous work [53], here we'll just give some expressions not explicitly given there which we'll use in the recount of this research. After EWSB the Z_2 even scalars acquire vacuum expectation values (vev) v_1 , v_2 and v_s , but from the consistency of the minimization conditions of the scalar potential two of the vevs are aligned $v_1 = \sqrt{3}v_2$. This, together with the requirement $v = \sqrt{v_s^2 + 4v_2^2} = 246$ GeV, where v is the SM vev leads to only one independent vev parameter, we choose $\tan \theta = 2v_2/v_s$ as independent parameter in the numerical calculations. EWSB induces mixing between the Z_2 even scalars, the CP even ones mix through the matrix:

$$Z^h = \begin{pmatrix} \cos(\alpha) & 0 & \sin(\alpha) \\ 0 & 1 & 0 \\ -\sin(\alpha) & 0 & \cos(\alpha) \end{pmatrix} \begin{pmatrix} 1 & 0 & 0 \\ 0 & \frac{1}{2} & -\frac{\sqrt{3}}{2} \\ 0 & \frac{\sqrt{3}}{2} & \frac{1}{2} \end{pmatrix} \quad (5)$$

while the charged and CP-odd scalars mix respectively with the matrices:

$$Z^C = Z^A = \begin{pmatrix} \cos(\theta) \sin(\theta) & 0 & \sin^2(\theta) \\ 0 & 1 & 0 \\ -\cos(\theta) \sin(\theta) & 0 & \cos^2(\theta) \end{pmatrix} \begin{pmatrix} 1 & 0 & 0 \\ 0 & \frac{1}{2} & -\frac{\sqrt{3}}{2} \\ 0 & \frac{\sqrt{3}}{2} & \frac{1}{2} \end{pmatrix} \quad (6)$$

i.e. both matrices coincide. Explicit expressions for the mixing angle α and the masses of all the scalars can be found in [53], these are given in terms of the 15 free parameters of the model: $\lambda_1 - \lambda_8, \lambda_{10} - \lambda_{14}, \tan \theta$ and μ_2 (there are only 15 free parameters because we are assuming a simple form of the Yukawa matrices, see the above reference for details and justification). There are 10 physical scalars in the model, we use interchangeably the following two notations, \tilde{h}_k with $k = 1, 2, 3$ for the neutral scalars H, H_3 and h (i.e. $\tilde{h}_1 = H, \tilde{h}_2 = H_3$ and $\tilde{h}_3 = h$), \tilde{A}_k for the neutral pseudo-scalars G^0, A_3 and A , and \tilde{H}_k^\pm for the charged scalars G^\pm, H_3^\pm and H^\pm , and in the dark sector we have the fields h_a, A_a and H_a^\pm with h_a the DM candidate. Here G^0 and G^\pm are the Goldstone fields which must be taken into account when it is advantageous to work in Feynman gauge. The second notation is intended to facilitate comparison with the Two Higgs Doublet Model (THDM) since a subset of the field content of the $S3$ model resembles the corresponding content of the THDM. It is favorable to work with the set of physical masses of the scalars as independent variables alongside with the parameters $\mu_2, \lambda_{13}, \lambda_{14}, \tan \theta$ and α , so we invert the expressions for the masses obtaining:

$$\begin{aligned} \lambda_1 &= \left(\csc^2 \theta (9 \cos(2\alpha) (M_h^2 - M_H^2) + 9M_h^2 + 9M_H^2 + 18M_{H_3^\pm}^2 - 2M_{H_3}^2 - 18M_{H^\pm}^2) + 18M_{H^\pm}^2 \right) / (36v^2) \\ \lambda_2 &= \left(\csc^2 \theta (-M_{A_3}^2 + M_{H_3^\pm}^2 + M_A^2 - M_{H^\pm}^2) - M_A^2 + M_{H^\pm}^2 \right) / (2v^2) \\ \lambda_3 &= \csc^2 \theta (9M_{H^\pm}^2 \cos(2\theta) - 18M_{H_3^\pm}^2 + 8M_{H_3}^2 + 9M_{H^\pm}^2) / (36v^2) \\ \lambda_4 &= -2M_{H_3}^2 \csc \theta \sec \theta / (9v^2) \\ \lambda_5 &= \left(9 \sin(2\alpha) \csc \theta \sec \theta (M_H^2 - M_h^2) + 2M_{H_3}^2 \sec^2 \theta + 36M_{H^\pm}^2 \right) / (18v^2) \\ \lambda_6 &= \left(M_{H_3}^2 \sec^2 \theta + 9M_A^2 - 18M_{H^\pm}^2 \right) / (9v^2) \\ \lambda_7 &= \left(M_{H_3}^2 \sec^2 \theta - 9M_A^2 \right) / (18v^2) \\ \lambda_8 &= \sec^2 \theta \left(9 \cos(2\alpha) (M_H^2 - M_h^2) - 2M_{H_3}^2 \tan^2(\theta) + 9(M_h^2 + M_H^2) \right) / (36v^2) \\ \lambda_{10} &= 2(M_{H_a^\pm}^2 - \mu_2^2) \csc^2 \theta / v^2 \\ \lambda_{11} &= - \left(\lambda_{14} v^2 \cot^2 \theta - M_{h_a}^2 \csc^2 \theta - M_{A_a}^2 \csc^2 \theta + 2M_{H_a^\pm}^2 \csc^2 \theta \right) / v^2 \\ \lambda_{12} &= \left(\csc^2 \theta (M_{h_a}^2 - M_{A_a}^2) \right) / (2v^2) \end{aligned} \quad (7)$$

These expressions are useful because in the directed scan it is simpler to vary the masses to probe the regions we are interested the most.

2.2 Enhanced annihilating cross section

As explained in the introduction, in the region of large DM masses it is important to take into account the Sommerfeld enhancement of the annihilation cross section, specially since we will assume the DM sector quasi-degenerate in mass $M_{h_a} \simeq M_{A_a} \simeq M_{H_a^\pm}$. These type of corrections are mandatory to include since the perturbative calculation of this cross section violates unitarity bounds in the large DM mass limit already at the one loop order, as can be seen for example in the process of DM annihilation into a pair of gammas which does not happens at the tree level. Thus, higher order corrections are needed to predict correctly this observable. The dominant contributions of higher order are the ladder type diagrams where multiple exchanges of on-shell mediators take place before the actual annihilation of the DM pairs. A complete formulation for the treatment of

Sommerfeld corrections can be found e.g. in [60–62]; for our model we follow their handling as done for the IDM in [29] since both dark sectors are very much alike.

As a first step it is necessary to find out the effective NR potentials induced by the exchange of the different gauge bosons and scalars, this is most simply done by calculating the allowed tree level scattering amplitudes in the complete theory and directly take the NR limit on them; also importantly to remember is to rescale the fields in order to have the NR Hamiltonian in canonical form otherwise the correct dependence of the potentials on the DM mass won't be attained. Also, it is useful to display the potential as a matrix in a basis of two-particle states in accordance with the possible scattering amplitudes $h_a h_a \rightarrow \text{DMDM}$, $A_a A_a \rightarrow \text{DMDM}$ and $H_a^+ H_a^- \rightarrow \text{DMDM}$ where DMDM here means either of $h_a h_a$, $A_a A_a$ or $H_a^+ H_a^-$. Note that the first process here, on account of the mass quasi-degeneracy, can induce the other two as part of the multi-scattering “ladder” but those latter processes cannot happen on its own reflecting the fact that h_a , being the DM candidate, is the only DM particle of the model present today. Explicitly the basis of two-particle states is $\{h_a h_a, A_a A_a, H_a^+ H_a^-\}$ and the elements of the matrix potential in this basis are obtained from the Fourier transform of the NR amplitude, for instance:

$$V_{11}(r) = \frac{1}{4M_{h_a}^2} \int \frac{d^3q}{(2\pi)^3} e^{i\mathbf{q}\cdot\mathbf{r}} iA_{\text{NR}}^{2\text{-body}}(h_a h_a \rightarrow h_a h_a) \quad (8)$$

where r is the relative coordinate of the two-particle state; the prefactor $1/4M_{h_a}^2$ comes from the rescaling of the NR fields. In general, the two body amplitudes in momentum space $A_{\text{NR}}^{2\text{-body}}$ differ by a factor of $\sqrt{2}$ relative to the “raw” amplitude calculated from the tree level Feynman diagram due to symmetrization of the two particle state when it is formed by identical particles in the initial state and distinguishable particles in the final state or vice versa. To understand these factors it is useful to visualize these amplitudes in the equivalent basis $\{h_a h_a, A_a A_a, H_a^+ H_a^-, H_a^- H_a^+\}$ where the last two states are treated as different; the equivalency of both basis is discussed in [63] in the context of the MSSM.

In this manner we obtain for the potential matrix:

$$V(r) = V_1(r) + V_2(r) \quad (9)$$

$$V_1(r) = \begin{pmatrix} \frac{-|s_{\tilde{h}_k}^{h_a h_a}|^2 e^{-M_{\tilde{h}_k} r}}{16\pi M_{h_a}^2 r} & \frac{-|s_{\tilde{A}_k}^{h_a A_a}|^2 e^{-M_{\tilde{A}_k} r}}{16\pi M_{h_a}^2 r} & \frac{-|s_{\tilde{H}_k^\pm}^{h_a H_a^\pm}|^2 e^{-M_{\tilde{H}_k^\pm} r}}{16\pi M_{h_a}^2 r} \\ \frac{-|s_{\tilde{A}_k}^{h_a A_a}|^2 e^{-M_{\tilde{A}_k} r}}{16\pi M_{h_a}^2 r} & \frac{-|s_{\tilde{h}_k}^{A_a A_a}|^2 e^{-M_{\tilde{h}_k} r}}{16\pi M_{h_a}^2 r} + 2(M_{A_a} - M_{h_a}) & \frac{-|s_{\tilde{H}_k^\pm}^{A_a H_a^\pm}|^2 e^{-M_{\tilde{H}_k^\pm} r}}{16\pi M_{h_a}^2 r} \\ \frac{-|s_{\tilde{H}_k^\pm}^{h_a H_a^\pm}|^2 e^{-M_{\tilde{H}_k^\pm} r}}{16\pi M_{h_a}^2 r} & \frac{-|s_{\tilde{H}_k^\pm}^{A_a H_a^\pm}|^2 e^{-M_{\tilde{H}_k^\pm} r}}{16\pi M_{h_a}^2 r} & \frac{-|s_{\tilde{h}_k}^{H_a^\pm H_a^\pm}|^2 e^{-M_{\tilde{h}_k} r}}{16\pi M_{h_a}^2 r} + 2(M_{H_a^\pm} - M_{h_a}) \end{pmatrix} \quad (10)$$

$$V_2(r) = \begin{pmatrix} 0 & -\frac{g_2^2 e^{-M_Z r}}{16\pi c_w^2 r} & -\frac{g_2^2 e^{-M_W r}}{16\pi r} \\ -\frac{g_2^2 e^{-M_Z r}}{16\pi c_w^2 r} & 0 & -\frac{g_2^2 e^{-M_W r}}{16\pi r} \\ -\frac{g_2^2 e^{-M_W r}}{16\pi r} & -\frac{g_2^2 e^{-M_W r}}{16\pi r} & -\frac{g_2^2 (s_w^2 + (1-2s_w^2)^2) e^{-M_Z r}}{16\pi c_w^2 r} \end{pmatrix} \quad (11)$$

with implicit sums over k and we have included the terms corresponding to the mass splittings; in the numerical calculation we will vary the two mass gaps as free parameters instead of the masses M_{A_a} , and $M_{H_a^\pm}$. Here g_2 is the weak coupling constant, $s_w = \sin\theta_w$, $c_w = \cos\theta_w$ with θ_w the Weinberg angle and the couplings are of the form:

$$\begin{aligned}
s_{\tilde{h}_k}^{h_a h_a} &= -i[v \sin \theta (\lambda_{10} + \lambda_{11} + \lambda_{12})(\sqrt{3}Z_{k2}^h + Z_{k3}^h)/2 + v \cos \theta \lambda_{14} Z_{k1}^h] \\
s_{\tilde{h}_k}^{A_a A_a} &= -i[v \sin \theta (\lambda_{10} + \lambda_{11} - 2\lambda_{12})(\sqrt{3}Z_{k2}^h + Z_{k3}^h)/2 + v \cos \theta \lambda_{14} Z_{k1}^h] \\
s_{\tilde{h}_k}^{H_a^\pm H_a^\pm} &= -i\lambda_{10} v \sin \theta (\sqrt{3}Z_{k2}^h + Z_{k3}^h)/2 \\
s_{\tilde{A}_k}^{h_a A_a} &= -2i\lambda_{12} v \sin \theta (\sqrt{3}Z_{k2}^A + Z_{k3}^A)/2 \\
s_{\tilde{H}_k}^{h_a H_a^\pm} &= (-i/2)[\lambda_{14} v \cos \theta Z_{k1}^C + v \sin \theta (2\lambda_{12} + \lambda_{11})(\sqrt{3}Z_{k2}^C + Z_{k3}^C)/2] \\
s_{\tilde{H}_k}^{A_a H_a^\pm} &= (-i/2)[\lambda_{14} v \cos \theta Z_{k1}^C + v \sin \theta (-2\lambda_{12} + \lambda_{11})(\sqrt{3}Z_{k2}^C + Z_{k3}^C)/2]
\end{aligned} \tag{12}$$

With the matrix potential at hand, a Schrödinger like system of equations for the deformed wave function [61] is solve numerically. Here we follow [64] where an equivalent equation with advantageous numerical properties is put forward:

$$h'(r) + h^2(r) + \frac{1}{4}M_{h_a}^2 v_{\text{rel}}^2 - M_{h_a} V(r) = 0 \tag{13}$$

with the matrix $h(r)$ satisfying the boundary condition

$$h(\infty) = (iM_{h_a} v_{\text{rel}}/2) \sqrt{1 - 4V(\infty)/(M_{h_a} v_{\text{rel}}^2)} \tag{14}$$

where $v_{\text{rel}} \sim 2 \times 10^3$ is the present day relative velocity of annihilating DM. The column vector defined as $d \equiv (d_{11} d_{12} d_{13})^T$ contains the Sommerfeld factors which are calculated from the relation:

$$dd^\dagger = \frac{1}{iM_{h_a} v_{\text{rel}}} (h(0) - h^\dagger(0)) \tag{15}$$

the matrix dd^\dagger has only one nonzero eigenvalue corresponding to its eigenvector d , note that this eigenvalue is just the modulus square of d . In figure 1 (b) we show the variation of the Sommerfeld factors with the DM mass, other free parameters are taken as in the benchmark or Best Fit Point (BFP) of section 5. We note that the three factors become slightly negative and close to zero around a DM mass of ~ 2.3 TeV, suggesting that around these values of parameter space a marked destructive interference is at work. On the other hand, for masses below 5 TeV the maximum occurs around ~ 2.1 TeV, with another local maximum close to ~ 3 TeV, with enhancements not surpassing a factor of ten. The BFP does not occurs in the vicinity of the highest enhancements and thus other important physical constraints weight in to shift it to a higher mass. In figure 1 (a) we also present the differential flux for the BFP as computed in the next section, including the Sommerfeld corrections.

The enhanced cross sections are then obtained with the aid of the Optical Theorem which relates the Forward Scattering Amplitude with the (tree level) annihilating amplitudes of the DM particles in the multiplet (for full details see the above references). The annihilating cross section in the limit of zero relative velocity for a given final state f is given by:

$$\sigma v_{\text{rel}}(h_a h_a \rightarrow f) = \frac{1}{2} (D\Gamma^f D^\dagger)_{11} \tag{16}$$

where $\Gamma = \sum_f \Gamma^f$ is the total matrix of absorptive terms to all final states f , and D is the matrix whose only nonzero row (in our basis the first row) is d^T . The elements of Γ^f are given explicitly by

$$\Gamma_{ij}^f = \frac{N_i N_j}{4M_{h_a}^2} \int \prod_{a \in f} \frac{d^3 q_a}{(2\pi)^3 2E_a} \mathcal{M}(i \rightarrow f) \mathcal{M}^*(j \rightarrow f) (2\pi)^4 \delta^4(p_i - p_j) \tag{17}$$

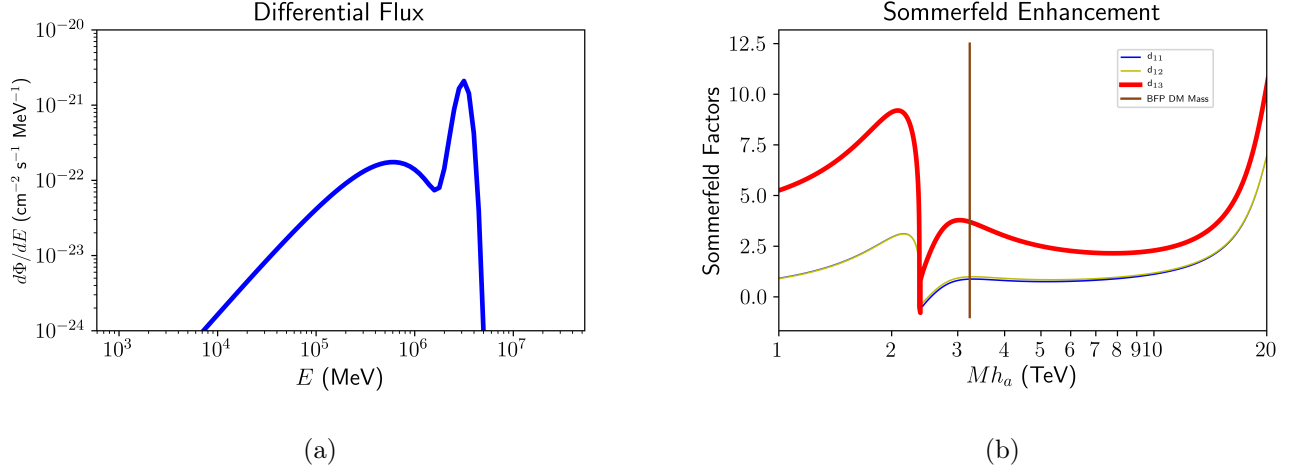


Figure 1: (a) Differential flux from DM pair annihilation (eq. 21) for the benchmark point of the model computed in section 5. (b) Sommerfeld enhancing factors as a function of the DM candidate mass, other parameters are taken as in the benchmark point. The vertical line signals the value of the benchmark DM mass.

here the indexes i and j refer to any element of the two-particle basis (the annihilating pair), f is any allowed final state of non-DM particles in the model, p_i and p_j are the 4-momenta of the initial and final states and the symmetry factors are given by $N_{h_a h_a} = N_{A_a A_a} = 1/\sqrt{2}$ and $N_{H_a^+ H_a^-} = 1$, with \mathcal{M} the tree level corresponding annihilating amplitudes.

We compute Γ^f for the following final states: $\gamma\gamma$, γZ , ZZ , W^+W^- , HH , H_3H_3 , hh and Hh (for HH_3 and H_3h , Γ^f is zero). For example, $\Gamma^{H_3H_3}$ is given by:

$$\Gamma^{H_3H_3} = \frac{1}{32\pi M_{h_a}^2} \begin{pmatrix} \frac{1}{2}\lambda_+^2 & \frac{9}{2}\lambda_- \lambda_+ & \frac{9}{\sqrt{2}}\lambda_{10}\lambda_+ \\ \frac{9}{2}\lambda_- \lambda_+ & \frac{1}{2}\lambda_-^2 & \frac{9}{\sqrt{2}}\lambda_{10}\lambda_- \\ \frac{9}{\sqrt{2}}\lambda_{10}\lambda_+ & \frac{9}{\sqrt{2}}\lambda_{10}\lambda_- & \lambda_{10}^2 \end{pmatrix} \quad (18)$$

where $\lambda_{\pm} \equiv \lambda_{10} + \lambda_{11} \pm 2\lambda_{12}$. Note that for this calculations we approximate the DM mass splittings as zero and we also neglect terms of the form M_X/M_{h_a} with X any gauge boson or scalar, for the numerical calculation we thus will keep the masses of the scalars to relatively light values. We list in appendix A the rest of the matrices.

2.3 Flux

The total differential cross section into gammas is given by

$$\frac{d\sigma_{\text{rel}}}{dE_{\gamma}} = \sum_f \sigma_{\text{rel}}(h_a h_a \rightarrow f) \times \frac{dN^f}{dE_{\gamma}} \quad (19)$$

Following [29], for the case of continuous yields ($f = \text{EW}$ or scalar boson pair as final state) we use the parametrization [65]:

$$\frac{dN^f}{dE_{\gamma}} = (0.73/M_{h_a}) x^{1.5} \exp\{-7.8x\} \quad (20)$$

with $x = E\gamma/M_{h_a}$. For the $\gamma\gamma$ or the γZ final states the yield is a Dirac delta centered respectively at M_{h_a} or $M_{h_a} - M_Z^2/(4M_{h_a})$. We model the delta as a Gaussian centered at the corresponding energy and of width equal to (conservatively) 15% the energy of the line, this since a delta would be a “monochromatic line” which in the context of ID experiments refers to spectral features with energy width much smaller than the energy resolution of the detector, typically 15% is achieved e.g. in HESS and therefore such value would be conservative for the CTA. Thus, with Gaussian width $= 0.15 M_{h_a}$: $(dN/dE\gamma)^{\gamma\gamma} = 2\delta(E\gamma - M_{h_a}) = 2(2.66/M_{h_a}) \exp(-22.22(x - M_{h_a})^2/M_{h_a}^2)$ and similar for γZ .

Finally, the predicted gamma ray flux from annihilation of DM particles is given by the expression:

$$\frac{d\Phi_\gamma}{dE_\gamma} = \frac{1}{4\pi} \left(\int_{\Delta\Omega} d\Omega \int_{l.o.s} ds \rho_\chi^2 \right) \left[\frac{1}{2M_{h_a}^2} \sum_f \sigma v_{\text{rel}}(h_a h_a \rightarrow f) \frac{dN^f}{dE_\gamma} \right] \quad (21)$$

here we have deliberately separated the equation into two parts, since the computation involved for each part is of very different nature. The first part (the astrophysical part) is well established for example in the case of dwarf spheroidal galaxies from astrophysical observations and it is known as the “J-factor”, we will take the dwarf as a point source with constant J-factor of $\log_{10} J = 19.52$ (with J in $\text{GeV}^2 \text{cm}^{-5}$) [66]. With the analysis of the previous section and the expressions for the yields given above we complete the second part and the flux prediction from the model.

3 Likelihood estimate

We choose to make our analysis based on a simulation of future observations of the dwarf spheroidal (dSph) galaxy Coma Berenices (or Coma) by the Cherenkov Telescope Array (southern hemisphere branch). Coma Berenices was discovered in 2006 by the Sloan Digital Sky Survey [67] and is a faint Milky Way satellite at a distance of 44 kpc from the Sun with right ascension of 12 h 26 min 59 sec and declination of 23 deg 54 min 15 sec; it is estimated to have a J -factor of $\log_{10} J = 19.52$, J in $\text{GeV}^2 \text{cm}^{-5}$ [66]. dSph galaxies are recurrent targets for searches of DM signals in ID experiments by virtue of their large inferred DM density and no known natural sources of gamma rays, Coma for example was part of a recent study of several dSphs in a DM signal search from HESS [68]; here, we try to follow their general analysis strategy in as much as possible as the available public tools allow us.

We simulate an observation run of Coma of 20 hours with the southern hemisphere CTA array in which we further assume a no-result experiment, in other words we assume that no significant excess of gamma rays above nominal background is found throughout the observation period. This will allow us to predict, based on current estimations of CTA’s expected baseline performance, exclusion limits on the parameter space of this particular model. We perform our analysis employing the reflected background technique [69] where the position of the telescope aim is slightly offset from the objective, the latter defined as a circular region (the On region) centered around Coma from which the simulated observation is used to fit against the predicted flux from the model. To compute the background in this technique several twin regions (the Off regions) are defined in symmetrical positions around the telescope aim (see figure 2) from which the background rate is extracted from the public Instrument Response Function (IRF) provided by the CTA Consortium. Background rates are expected to be fairly symmetric with respect to the position of the camera aim and thus this method minimizes a possible source of systematic errors from modeling the background from Monte Carlo simulations.

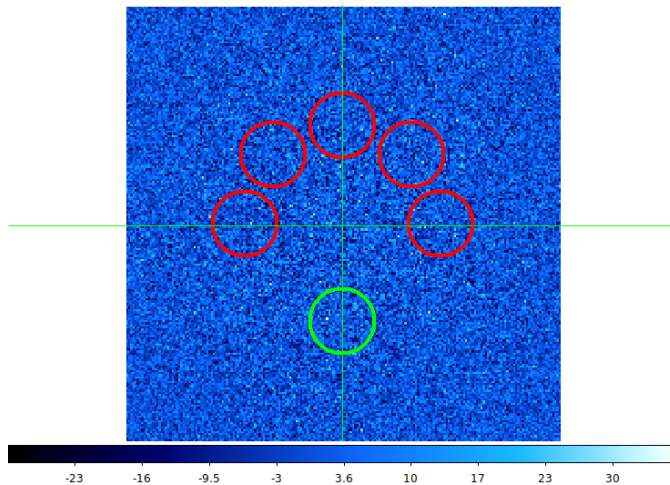


Figure 2: On and Off-regions for the observation of the Coma Berenices spherical dwarf and the determination of the background. The dwarf is located in the center of the green circle at the bottom, and five adjacent regions (red circles) located in symmetric points with respect to the observation point are used to determine the background signal, the telescope aim is located at the center of the intersecting lines. The color axis represents the signal detection significance, the absence of notorious bright spots in the region means that no known sources of gamma rays need to be taken into account in the determination of the background.

In an On/Off analysis the model M is composed of the signal (predicted number of gamma rays) and the background $M = M_s + M_b$, the background model M_b is taken from the background information provided in the IRF and the signal M_s is calculated from the predicted differential gamma ray flux. The likelihood estimate is constructed from the formula:

$$-\log \mathcal{L}(M) = \sum_i s_i(M_s) + a_i(M_b)b_i(M_b) - n_i^{\text{on}} \log[s_i(M_s) + a_i(M_b)b_i(M_b)] + b_i(M_b) - n_i^{\text{off}} \log b_i(M_b) \quad (22)$$

where n_i^{on} (n_i^{off}) is the number of events in bin i of the On (Off) region, $s_i(M_s)$ ($b_i(M_b)$) is the number of expected signal (background) counts in bin i of the On (Off) region and $a_i(M_b)$ is the ratio between the spatial integral over the background model in the On region and the Off region for bin i .

The detection significance of the model is estimated using the Test Statistic (TS) which is defined as:

$$\text{TS} = 2[\log \mathcal{L}(M_s + M_b) - \log \mathcal{L}(M_b)] \quad (23)$$

which involves the log-likelihood value obtained when fitting the model and the background together to the simulated data, and also the log-likelihood value when fitting only the background.

Note that for the calculation of these quantities all the parameters of the theoretical model remain fixed because the construction of the likelihood profile is done by an external (to the CTA tools) minimizer which in each step provides a set of model parameter values along with the predicted differential flux, requests the value of the CTA likelihood function (from the CTA tools), computes additional likelihood components and based on this information moves around in parameter space searching for the maximum of the total likelihood function, as explained in the next section.

4 Numerical analysis

The setup for the numerical computation is very simple, we define a function F which accepts as input a set of values for the free parameters of the model and returns the value of the total likelihood function. The problem is then reduced to the maximization of this function, for this we use `Diver` [70] in standalone mode, the differential evolution scanner available in the `Gambit` [71] package, and for post-processing of the resulting data sets we use `Pippi` [72]. To reduce the number of free parameters of the model in the scan we fix the value of the scalar h to the Higgs mass [73, 74], for simplicity we fix $\lambda_{13} = 0.001$ to easily satisfy inequalities that ensure no tunneling to vacua that breaks the Z_2 discrete symmetry [20], and we take μ_2^2 given in terms of the DM mass ($M_{h_a}^2 - \mu_2^2$ small constant) so that the gaps $M_{H_a^\pm} - M_{h_a}$ and $M_{A_a} - M_{h_a}$ can be taken relatively small in order to explore regions that presumably have big enhancement factors of the annihilation cross section. For the same reason, we take the masses of the heavy scalars in-between 200 and 800 GeV, since the larger the masses of these particles the minor the contribution to the deforming potential in the Sommerfeld factor.

The layout of F is a little bit more technically challenging though. Basically we divide points of the model’s parameter space into two categories, the ones that satiate the physical constraints and the ones that doesn’t. In the latter case we don’t discard the points, instead equivalently, we assign a bad likelihood to them. Construction of the constraint filters is done with the aid of several public tools: we implement the model in `SARAH` [75–78] from which we generate corresponding model files for the rest of the tools. Tree level LQT [79] and finite energy [80] unitarity conditions are calculated with the `SARAH-SPheno` [81–83] framework, and we check current experimental limits from Higgs and heavy scalar searches using `HiggsBounds` [84–88]. For a more complete description of the implementation of the constraints see our previous work [53].

Next we compute the Sommerfeld factors (15) by solving the corresponding coupled equations (13) by means of a fourth-order Rosenbrock method [89], the non-relativistic potentials, scattering and annihilation amplitudes are obtained with the aid of `FeynArts` [90], `FormCalc` [91] and `FeynCalc` [92–94]. This allow us to calculate the enhanced annihilation cross sections from which we compute the differential gamma ray flux using (21).

From the predicted differential flux a file with energy and differential flux columns is created which is then fed to `ctools` [95, 96], the public software package for the scientific analysis of Cherenkov Telescope Array data and simulations. With the aid of `ctools`, an On/Off analysis of the model is performed along the lines described in the previous section deriving one piece of the likelihood value up to this point. We treat Coma as a point-like source and the size of the on and off regions are taken to be 0.3 degrees in radius. We note that this part of the calculation is the most expensive in terms of computational time, with so much free parameters and taking into account that a total of approximately 4.5×10^7 F -function evaluations are needed for the algorithm to converge and find the absolute maximum of the likelihood function, this makes the inclusion of more than one dwarf in the analysis unpractical with the computational resources at hand,² because the position of the dwarfs in the sky are very different and an independent analysis for each one of them has to be done and therefore the time expended in each dwarf would be the same, increasing linearly the total time of the run.

Finally the computation of the value of the relic abundance is made with the aid of `Micr-OMEGAS` [97]. To allow for the possibility of under-abundant DM candidate we penalize only relic abundance values above the Planck experimental measured interval [98], points with a value of this

²In addition, several runs incrementing the population of the minimizer are necessary to ensure that proper convergence to the global maximum is attained [70].

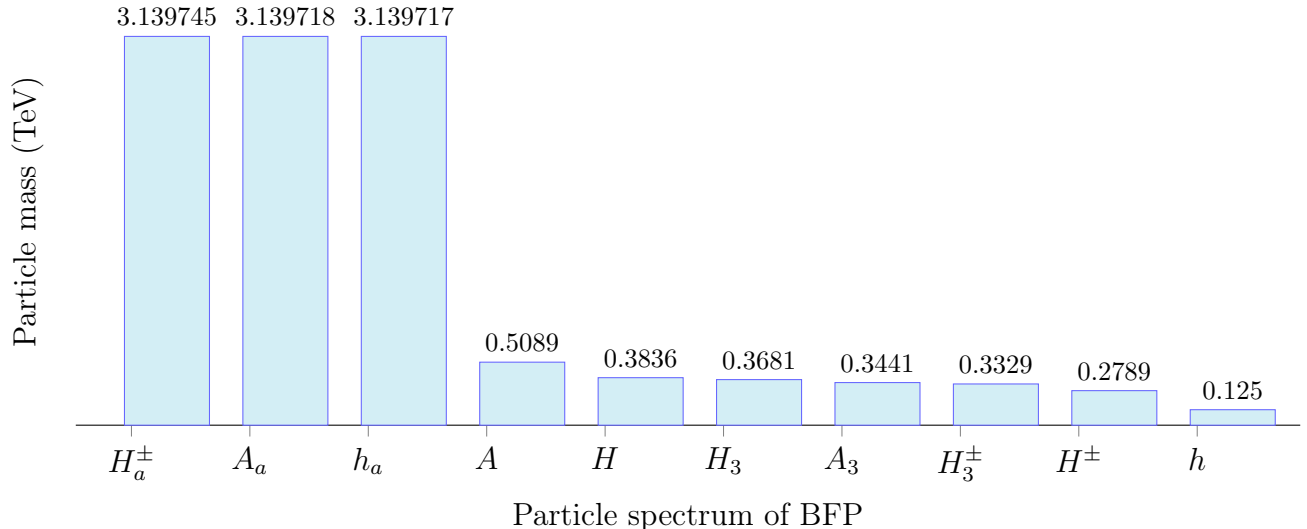


Figure 3: Spectrum of masses of the scalar particles in the model evaluated at the BFP.

observable conforming to or below the Planck value are assigned a likelihood value of $1/(\sqrt{2\pi}\sigma)$ with σ the Planck measured interval, this likelihood value is added to the previously calculated one.

More technical details of the procedure described here can be found in the source codes of the modules used to generate the results of this research, see [99].

5 Results

We report here our results obtained from a final run with a population of 40 thousand points for the minimizer. The spectrum of masses of the scalar sector at the best fit point is presented in figure 3, the DM sector masses are intentionally kept quasi-degenerate in order to facilitate the occurrence of the Sommerfeld effect by allowing the production of on-shell DM intermediate states other than h_a (by keeping the DM mass gaps small), we find that the heavy (non DM) scalars lie with masses in between 278 and 509 GeV.

In figure 4 bottom panel, we present a scatter plot of points in the parameter space of the model and their predictions of the value of the relic abundance as a function of the mass of the DM candidate, the points are color coded according to whether or not they satisfy all physical constraints. With navy blue points excluded from heavy scalar experimental searches, the rest of the points satisfy this constraint as well as unitarity and stability and thus this plot makes it clear that only the region below the Planck value (the horizontal line) represents physically acceptable points (assuming also the possibility of an under-abundant DM candidate). Therefore, the region with DM masses above ~ 5 TeV is clearly excluded. The difference between the light blue points and the red ones is that for the latter the scalar h is within the decoupling limit and thus has all the characteristics of the SM Higgs particle. In addition, green points (a subset of the red ones) predict a relic abundance within the experimental Planck interval, note that we found this kind of points within a region approximately from ~ 1.3 to ~ 4.9 TeV masses.

In the middle panel of figure 4 we present a scatter plot of the annihilation cross section versus the DM candidate mass with the same color code for the points as above. We include in the plot two exclusion curves from independent analysis. The first, labeled Coma (HESS), is an analysis of the Coma Dwarf from observations with the HESS Imaging Atmospheric Cherenkov Telescopes [68] and

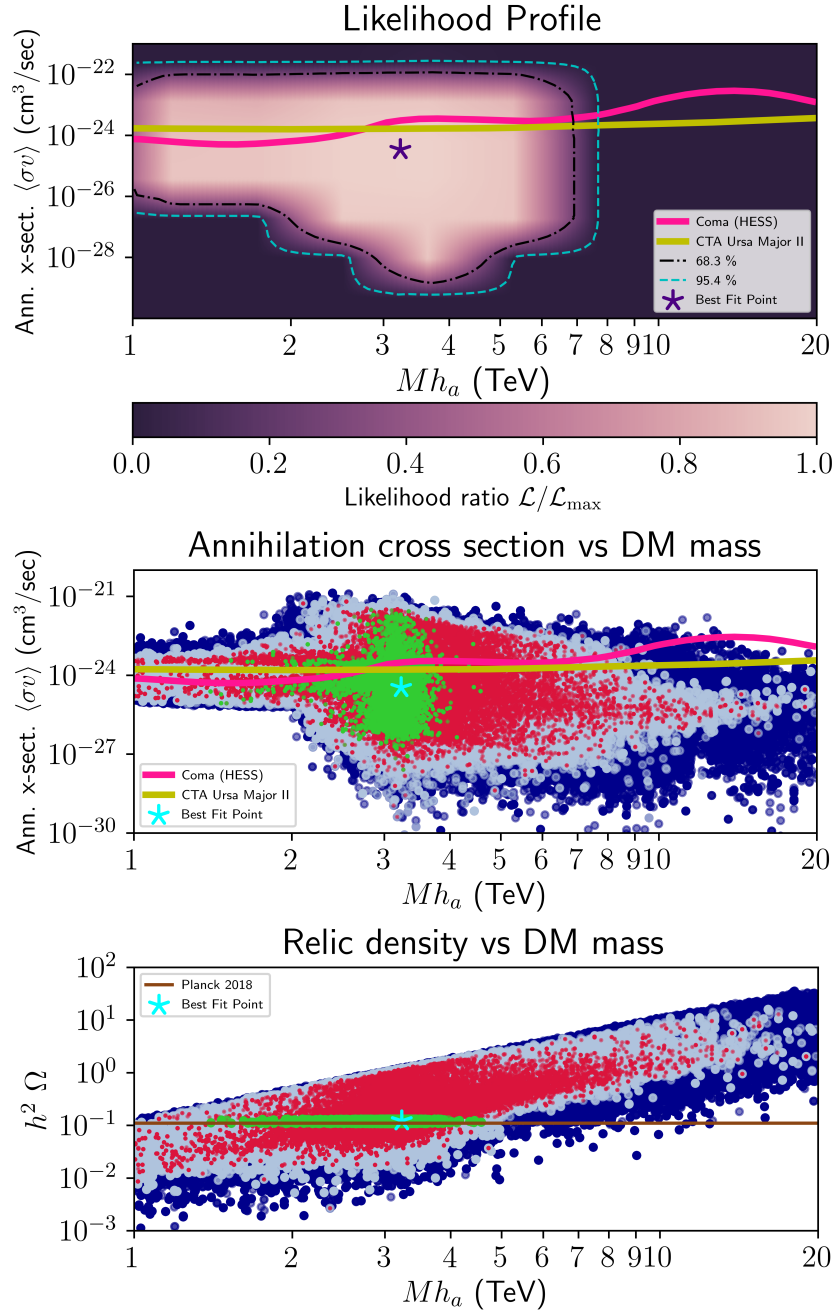


Figure 4: (Color online) Top panel: Normalized likelihood profile as a function of the zero-velocity averaged annihilation cross section and the DM candidate mass. Contours for a coverage probability of 68.3% and 95.4% for two degrees of freedom are shown as dot dashed and dashed respectively, and the BFP is marked as a star. For comparison we show exclusion curves from an analysis of an observation of Coma by HESS [68] and a simulation of a CTA observation of Ursa Major II [100] (both model independent analysis). Middle panel: Scatter plot of the annihilation cross section as a function of the DM mass, navy blue points are consistent with unitarity and stability bounds but are excluded from experimental scalar searches; light blue points are consistent with all of these constraints while the red points in addition satisfy the decoupling limit for h ; green points predict a relic abundance within the experimental Planck value [98]. Bottom panel: Scatter plot of the predicted relic abundance as a function of the DM mass, the color code of the points is the same as the middle panel.

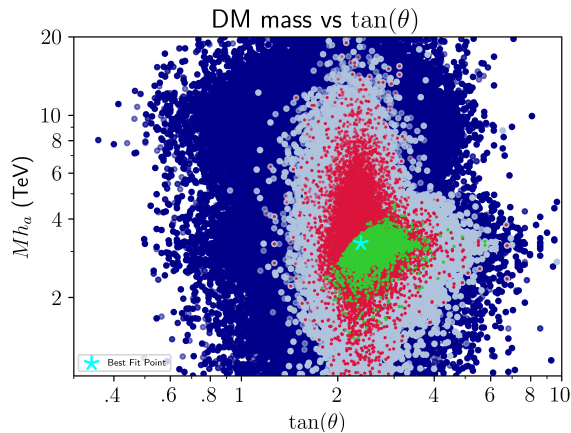


Figure 5: (Color online) Scatter plot of the DM mass as a function of $\tan \theta$, the color code of the points is as in figure 4.

represents a 95% C.L. exclusion limit on the velocity weighted cross section for DM self-annihilation into gamma ray lines ($\gamma\gamma$ lines). They also include combined analysis with other dwarfs but we chose to present the comparison only with the limits from the observations of Coma Berenices; note that this limits assume generic DM (or model independent). The second exclusion curve, labeled CTA Ursa Major II, is from a simulation of the CTA sensitivity to DM annihilation in the channel $DM DM \rightarrow W^+W^-$ assuming a 500 hour observation of the Ursa Major II dwarf [100], also for generic dark matter; while in this reference there are also limits from Coma Berenices (but only 50 hour observation simulation), we chose to compare with Ursa Major II because it has more stringent limits. We note from this scatter plot that there is a “depression” starting around masses of 2 TeV where the cross section begins to take smaller values, this may be indicative that the destructive interference in the enhancement factors found in the BFP (figure 1) in between 2 and 3 TeV values of the DM mass is a generic feature of the parameter space and not only of the BFP.

Next, in the top panel of figure 4 we present the normalized likelihood profile as a function of the annihilation cross section and the DM candidate mass, the best fit point of the analysis is marked as a star (in all panels); we note how the region above a DM mass of 5 TeV is gradually disfavored mostly because it is already ruled out by an overproduction of DM not consistent with observations. It is apparent from this plot that close to a third of the viable region of plausible physical points lie above the two exclusion curves which are very similar in the region of masses below 7 TeV, with the HESS limits slightly better below ~ 3 TeV and the CTA limits slightly better above this mass. Both exclusion curves come very close to disfavour the best fit point of the model, probably with an improvement of the limits by an order of magnitude the BFP could be excluded. Notice that we are assuming the possibility of under-abundant DM, had we imposed penalization of the likelihood function also for points below the Planck interval by the assumption that this DM candidate comprises the totality of the observed DM in the Universe, then the bright region of this plot would appear shrunken horizontally reflecting the fact that green points in the other plots lie mostly around a mass of ~ 3.1 TeV, as noted before.

In figure 5 we show an scatter plot of the DM mass candidate as a function of $\tan \theta$ with the color coding the same as in the previous scatter plots. We see clearly the approximately formation of subregions contained within regions of a lesser restraining level, thus points that satisfy the decoupling limit cover around two thirds of the region of points satisfying unitarity, stability and Higgs searches, while points predicting a relic abundance value within the experimental interval lie

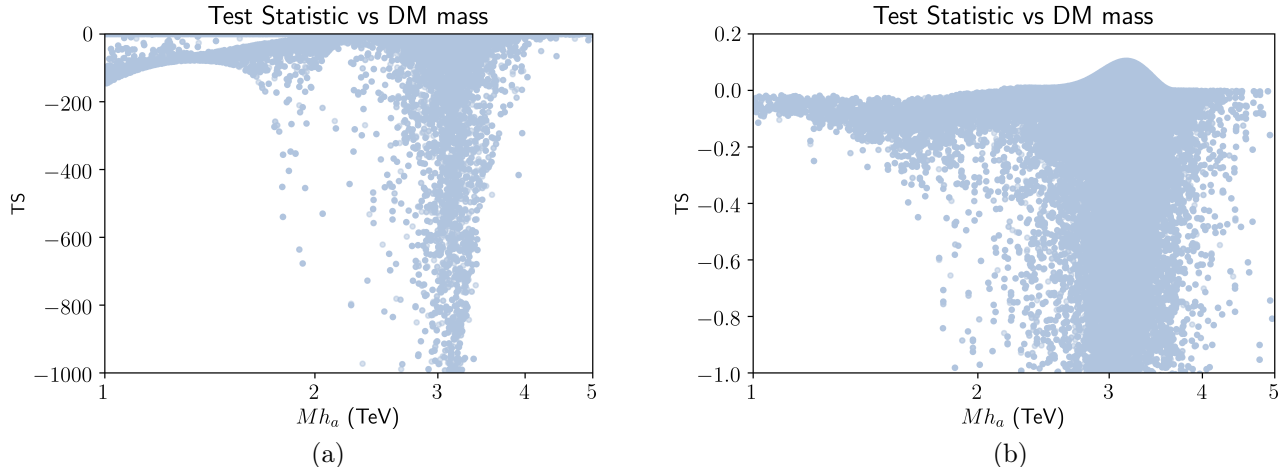


Figure 6: (a) Scatter plot of the Test Statistic as a function of the DM mass, all the points shown satisfy unitarity, stability and experimental higgs searches constraints and in addition predict a relic abundance within the experimental Planck value or below it. (b) Same as (a) but shows only values above a $TS > -1.0$.

mostly between values of $\tan\theta$ equal 2 and 4, with the BFP attaining a value of 2.34.

Since we are simulating a null-result experiment, the best indicator of the actual sensibility of the experiment would be the computation of the Test Statistic to compare to what is expected under the null hypothesis (no DM present), this technique is employed in current ID experiments to construct exclusion limits from their non-observation of significant gamma ray signals above the background. With this in mind, we present in figure 6 (a) the scatter plot of the TS as a function of the DM mass in the DM mass range between 1 and 5 TeV, this accounting for the fact that higher masses predict overproduction of DM in conflict with the observed abundance as was discussed before. In fact, during the computational runs the calculation of the CTA likelihood and the TS was not performed for points predicting a relic above the Planck interval. Instead, these points were automatically assigned a “bad” value of the likelihood for purposes of optimization of the code. Figure 6 (b) shows the same plot but only for $TS > -1.0$, here we note that the TS reaches an almost constant maximum value very close to zero for a given mass, with a small bulb around a DM mass of ~ 3.2 TeV, attaining a maximum TS close to 0.1.

For points in figure 6 lying in a (vertical) ray of constant DM mass, we consider the difference $TS_{\max} - TS \equiv \Delta TS$, since the Test Statistic approaches a χ^2 function in the large data sample limit, a value of $\Delta TS = 1$ corresponds to a coverage probability of 68.3% for estimation of 1 parameter [101], which we take as the annihilation cross section. Therefore, we interpret points in such a ray with $\Delta TS > 1$ as excluded with a C.L. of 68%. In this manner we construct a “Test Statistic profile”, shown in figure 7 as a function of the annihilation cross section and the DM mass. Since the value of TS_{\max} is very small, for points such that $\Delta TS \gtrsim 1$ we approximate $\Delta TS \approx |TS|$ and the limit condition becomes $|TS| > 1$ for them. Following these arguments, we consider the points in the upper region of this figure excluded by our analysis (at the corresponding C.L.) while the points in the bottom region are not. We can then interpret the boundary of the upper (green) region as an approximate exclusion curve, except that there is an overlapping of the two regions, which we take as a consequence of the error bars of the analysis, though a precise determination of these errors will not be pursued here.

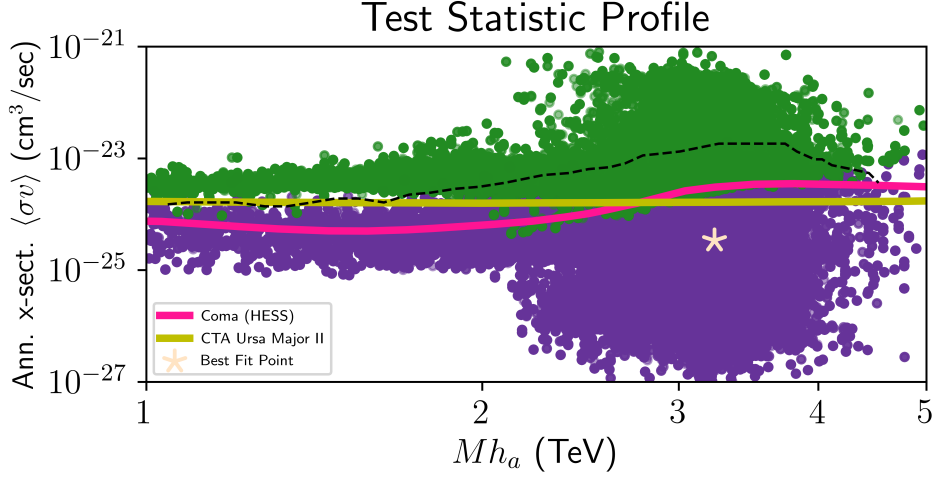


Figure 7: (Color online) Scatter plot of the annihilation cross section as a function of the DM mass with the points colored according to their value of the Test Statistic: purple points (mostly bottom region) have a TS less than 1 in absolute value, while green points (mostly top region) have a TS greater than 1 in absolute value. The exclusion curves are as in figure 4 and the dashed black line shows the extend to which the purple and the green points overlap (for more details see main text).

6 Conclusions

We have presented in this letter an analysis of the Dark $S3$ model in the region of high dark matter candidate mass pursuing a determination of the prospects of indirect detection specific to this model. In order to take into account most of the important theoretical predictions of the model we calculated the non-relativistic potentials which potentially can cause enhancements on the value of the annihilation cross section by means of the Sommerfeld effect. We computed the enhancement factors and the annihilation matrices leading to a proper determination of the cross sections and the differential gamma ray flux from annihilation of DM pairs in the Coma Berenices dwarf galaxy. We determined then the likelihood profile in parameter space from a simulation of observations of such dwarf galaxy at the CTA assuming a null-result experiment using available public tools. We conclude from our results that DM masses above 5 TeV are definitely exclude mainly because of overproduction of DM not consistent with the observed value of the relic abundance. For masses below 5 TeV the best fit point of the likelihood analysis suggest a DM value of ~ 3.14 TeV, somewhat higher than the value where the highest cross section enhancement occurs indicating that other constraints such as unitarity and scalar searches are also important for the precise determination of the best fit. Comparison of our results with independent analysis in the literature shows that current as well as estimated exclusion limits are close to disfavour the model's BFP, at least under the conditions of the present analysis. Perhaps the inclusion of a combined analysis taking into consideration several more dwarf galaxies will allow more stringent limits on the model.

A Absorptive terms

In this appendix we list the non-zero (symmetric) matrices of absorptive terms for the calculation of the enhanced annihilation DM cross section that complement equation (18).

Channel $\gamma\gamma$:

$$\Gamma^{\gamma\gamma} = \frac{e^4}{4\pi M_{h_a}^2} \times \text{diag}(0, 0, 1) \quad (24)$$

Channel γZ :

$$\Gamma^{\gamma Z} = \frac{e^4 \cot^2(2\theta_w)}{4\pi M_{h_a}^2} \times \text{diag}(0, 0, 1) \quad (25)$$

Channel ZZ :

$$\begin{aligned} \Gamma_{11}^{ZZ} &= \frac{1}{1024\pi M_{h_a}^2} (8g_2^4 \sec^4(\theta_w) + 4(-\cos(2\theta)(\lambda_+ - \lambda_{14}) + \lambda_+ + \lambda_{14})^2) \\ \Gamma_{12}^{ZZ} &= \frac{1}{512\pi M_{h_a}^2} (4g_2^4 \sec^4(\theta_w) - 4\cos(2\theta) ((\lambda_{10} + \lambda_{11})^2 - 4\lambda_{12}^2 - \lambda_{14}^2) + \cos(4\theta)(\lambda_+ - \lambda_{14})(\lambda_- - \lambda_{14}) \\ &\quad + 2\lambda_{14}(\lambda_{10} + \lambda_{11}) + 3(\lambda_{10} + \lambda_{11})^2 - 12\lambda_{12}^2 + 3\lambda_{14}^2) \\ \Gamma_{13}^{ZZ} &= \frac{1}{64\sqrt{2}\pi M_{h_a}^2} (g_2^4 \cos^2(2\theta_w) \sec^4(\theta_w) + \lambda_{10} \sin^2(\theta)(-\cos(2\theta)(\lambda_+ - \lambda_{14}) + \lambda_+ + \lambda_{14})) \\ \Gamma_{22}^{ZZ} &= \frac{1}{1024\pi M_{h_a}^2} (8g_2^4 \sec^4(\theta_w) + 4(-\cos(2\theta)(\lambda_- - \lambda_{14}) + \lambda_- + \lambda_{14})^2) \\ \Gamma_{23}^{ZZ} &= \frac{1}{64\sqrt{2}\pi M_{h_a}^2} (g_2^4 \cos^2(2\theta_w) \sec^4(\theta_w) + \lambda_{10} \sin^2(\theta)(-\cos(2\theta)(\lambda_- - \lambda_{14}) + \lambda_- + \lambda_{14})) \\ \Gamma_{33}^{ZZ} &= \frac{1}{64\pi M_{h_a}^2} (g_2^4 \cos^4(2\theta_w) \sec^4(\theta_w) + 2\lambda_{10}^2 \sin^4(\theta)) \end{aligned} \quad (26)$$

Channel W^+W^- :

$$\begin{aligned} \Gamma_{11}^{W^+W^-} &= \frac{1}{512\pi M_{h_a}^2} (4g_2^4 - 4\cos(2\theta)(\lambda_+ - \lambda_{14})(\lambda_+ + \lambda_{14}) + \cos(4\theta)(\lambda_+ - \lambda_{14})^2 \\ &\quad + 2\lambda_{14}(\lambda_+) + 3(\lambda_+)^2 + 3\lambda_{14}^2) \\ \Gamma_{12}^{W^+W^-} &= \frac{1}{512\pi M_{h_a}^2} (4g_2^4 - 4\cos(2\theta) ((\lambda_{10} + \lambda_{11})^2 - 4\lambda_{12}^2 - \lambda_{14}^2) + \cos(4\theta)(\lambda_+ - \lambda_{14})(\lambda_- - \lambda_{14}) \\ &\quad + 2\lambda_{14}(\lambda_{10} + \lambda_{11}) + 3(\lambda_{10} + \lambda_{11})^2 - 12\lambda_{12}^2 + 3\lambda_{14}^2) \\ \Gamma_{13}^{W^+W^-} &= \frac{1}{256\sqrt{2}\pi M_{h_a}^2} (4g_2^4 + \lambda_{10} \cos(4\theta)(\lambda_+ - \lambda_{14}) + \lambda_{10}(3(\lambda_+) + \lambda_{14}) - 4\lambda_{10} \cos(2\theta)\lambda_+) \\ \Gamma_{22}^{W^+W^-} &= \frac{1}{512\pi M_{h_a}^2} (4g_2^4 - 4\cos(2\theta)(\lambda_- - \lambda_{14})(\lambda_- + \lambda_{14}) + \cos(4\theta)(\lambda_- - \lambda_{14})^2 + 2\lambda_{14}(\lambda_-) \\ &\quad + 3(\lambda_-)^2 + 3\lambda_{14}^2) \\ \Gamma_{23}^{W^+W^-} &= \frac{1}{256\sqrt{2}\pi M_{h_a}^2} (4g_2^4 + \lambda_{10} \cos(4\theta)(\lambda_- - \lambda_{14}) + \lambda_{10}(3(\lambda_-) + \lambda_{14}) - 4\lambda_{10} \cos(2\theta)(\lambda_-)) \\ \Gamma_{33}^{W^+W^-} &= \frac{1}{256\pi M_{h_a}^2} (4g_2^4 + \lambda_{10}^2(\cos(4\theta) - 4\cos(2\theta)) + 3\lambda_{10}^2) \end{aligned} \quad (27)$$

Channel HH :

$$\begin{aligned} \Gamma_{11}^{HH} &= \frac{1}{64\pi M_{h_a}^2} ((\sin^2(\alpha)(\lambda_+) + \lambda_{14} \cos^2(\alpha))^2) \\ \Gamma_{12}^{HH} &= \frac{1}{64\pi M_{h_a}^2} (9 (\sin^2(\alpha)(\lambda_-) + \lambda_{14} \cos^2(\alpha)) (\sin^2(\alpha)(\lambda_+) + \lambda_{14} \cos^2(\alpha))) \\ \Gamma_{13}^{HH} &= \frac{1}{32\sqrt{2}\pi M_{h_a}^2} (9\lambda_{10} \sin^2(\alpha) (\sin^2(\alpha)(\lambda_+) + \lambda_{14} \cos^2(\alpha))) \\ \Gamma_{22}^{HH} &= \frac{1}{64\pi M_{h_a}^2} ((\sin^2(\alpha)(\lambda_-) + \lambda_{14} \cos^2(\alpha))^2) \\ \Gamma_{23}^{HH} &= \frac{1}{32\sqrt{2}\pi M_{h_a}^2} (9\lambda_{10} \sin^2(\alpha) (\sin^2(\alpha)(\lambda_-) + \lambda_{14} \cos^2(\alpha))) \\ \Gamma_{33}^{HH} &= \frac{1}{32\pi M_{h_a}^2} (\lambda_{10}^2 \sin^4(\alpha)) \end{aligned} \quad (28)$$

Channel hh :

$$\begin{aligned}
\Gamma_{11}^{hh} &= \frac{1}{64\pi M_{h_a}^2} ((\cos^2(\alpha)(\lambda_+) + \lambda_{14} \sin^2(\alpha))^2) \\
\Gamma_{12}^{hh} &= \frac{1}{64\pi M_{h_a}^2} (9 (\cos^2(\alpha)(\lambda_-) + \lambda_{14} \sin^2(\alpha)) (\cos^2(\alpha)(\lambda_+) + \lambda_{14} \sin^2(\alpha))) \\
\Gamma_{13}^{hh} &= \frac{1}{32\sqrt{2}\pi M_{h_a}^2} (9\lambda_{10} \cos^2(\alpha) (\cos^2(\alpha)(\lambda_+) + \lambda_{14} \sin^2(\alpha))) \\
\Gamma_{22}^{hh} &= \frac{1}{64\pi M_{h_a}^2} ((\cos^2(\alpha)(\lambda_-) + \lambda_{14} \sin^2(\alpha))^2) \\
\Gamma_{23}^{hh} &= \frac{1}{32\sqrt{2}\pi M_{h_a}^2} (9\lambda_{10} \cos^2(\alpha) (\cos^2(\alpha)(\lambda_-) + \lambda_{14} \sin^2(\alpha))) \\
\Gamma_{33}^{hh} &= \frac{1}{32\pi M_{h_a}^2} (\lambda_{10}^2 \cos^4(\alpha))
\end{aligned} \tag{29}$$

Channel Hh :

$$\begin{aligned}
\Gamma_{11}^{Hh} &= \frac{1}{64\pi M_{h_a}^2} (\sin^2(\alpha) \cos^2(\alpha) (\lambda_+ - \lambda_{14})^2) \\
\Gamma_{12}^{Hh} &= \frac{1}{64\pi M_{h_a}^2} (9 \sin^2(\alpha) \cos^2(\alpha) (\lambda_- - \lambda_{14}) (\lambda_+ - \lambda_{14})) \\
\Gamma_{13}^{Hh} &= \frac{1}{32\sqrt{2}\pi M_{h_a}^2} (9\lambda_{10} \sin^2(\alpha) \cos^2(\alpha) (\lambda_+ - \lambda_{14})) \\
\Gamma_{22}^{Hh} &= \frac{1}{64\pi M_{h_a}^2} (\sin^2(\alpha) \cos^2(\alpha) (\lambda_- - \lambda_{14})^2) \\
\Gamma_{23}^{Hh} &= \frac{1}{32\sqrt{2}\pi M_{h_a}^2} (9\lambda_{10} \sin^2(\alpha) \cos^2(\alpha) (\lambda_- - \lambda_{14})) \\
\Gamma_{33}^{Hh} &= \frac{1}{32\pi M_{h_a}^2} (\lambda_{10}^2 \sin^2(\alpha) \cos^2(\alpha))
\end{aligned} \tag{30}$$

Acknowledgements

This research has made use of the CTA instrument response functions (version prod3b-v2) provided by the CTA Consortium and Observatory (for more details see [102]), as well as the ctools package [95, 96], a community-developed analysis package for Imaging Air Cherenkov Telescope data. ctools is based on GammaLib, a community-developed toolbox for the scientific analysis of astronomical gamma-ray data. Figure 2 was made with the aid of SAOImage DS9 [103]. C.E. acknowledges the support of Conacyt (México) Cátedra 341. This research is partly supported by UNAM PAPIIT through Grant IN111518.

References

- [1] G. C. Branco et al. “Theory and phenomenology of two-Higgs-doublet models”. In: *Phys. Rept.* 516 (2012), pp. 1–102. DOI: [10.1016/j.physrep.2012.02.002](https://doi.org/10.1016/j.physrep.2012.02.002). arXiv: [1106.0034](https://arxiv.org/abs/1106.0034) [hep-ph].
- [2] Nilendra G. Deshpande and Ernest Ma. “Pattern of Symmetry Breaking with Two Higgs Doublets”. In: *Phys. Rev. D* 18 (1978), p. 2574. DOI: [10.1103/PhysRevD.18.2574](https://doi.org/10.1103/PhysRevD.18.2574).
- [3] John McDonald. “Gauge singlet scalars as cold dark matter”. In: *Phys. Rev. D* 50 (1994), pp. 3637–3649. DOI: [10.1103/PhysRevD.50.3637](https://doi.org/10.1103/PhysRevD.50.3637). arXiv: [hep-ph/0702143](https://arxiv.org/abs/hep-ph/0702143) [HEP-PH].
- [4] Ernest Ma. “Verifiable radiative seesaw mechanism of neutrino mass and dark matter”. In: *Phys. Rev. D* 73 (2006), p. 077301. DOI: [10.1103/PhysRevD.73.077301](https://doi.org/10.1103/PhysRevD.73.077301). arXiv: [hep-ph/0601225](https://arxiv.org/abs/hep-ph/0601225) [hep-ph].
- [5] Riccardo Barbieri, Lawrence J. Hall, and Vyacheslav S. Rychkov. “Improved naturalness with a heavy Higgs: An Alternative road to LHC physics”. In: *Phys. Rev. D* 74 (2006), p. 015007. DOI: [10.1103/PhysRevD.74.015007](https://doi.org/10.1103/PhysRevD.74.015007). arXiv: [hep-ph/0603188](https://arxiv.org/abs/hep-ph/0603188) [hep-ph].

- [6] Laura Lopez Honorez et al. “The Inert Doublet Model: An Archetype for Dark Matter”. In: *JCAP* 0702 (2007), p. 028. DOI: [10.1088/1475-7516/2007/02/028](https://doi.org/10.1088/1475-7516/2007/02/028). arXiv: [hep-ph/0612275](https://arxiv.org/abs/hep-ph/0612275) [[hep-ph](#)].
- [7] Debasish Majumdar and Ambar Ghosal. “Dark Matter candidate in a Heavy Higgs Model - Direct Detection Rates”. In: *Mod. Phys. Lett. A* 23 (2008), pp. 2011–2022. DOI: [10.1142/S0217732308025954](https://doi.org/10.1142/S0217732308025954). arXiv: [hep-ph/0607067](https://arxiv.org/abs/hep-ph/0607067) [[hep-ph](#)].
- [8] Thomas Hambye and Michel H. G. Tytgat. “Electroweak symmetry breaking induced by dark matter”. In: *Phys. Lett. B* 659 (2008), pp. 651–655. DOI: [10.1016/j.physletb.2007.11.069](https://doi.org/10.1016/j.physletb.2007.11.069). arXiv: [0707.0633](https://arxiv.org/abs/0707.0633) [[hep-ph](#)].
- [9] Michael Gustafsson et al. “Significant Gamma Lines from Inert Higgs Dark Matter”. In: *Phys. Rev. Lett.* 99 (2007), p. 041301. DOI: [10.1103/PhysRevLett.99.041301](https://doi.org/10.1103/PhysRevLett.99.041301). arXiv: [astro-ph/0703512](https://arxiv.org/abs/astro-ph/0703512) [[ASTRO-PH](#)].
- [10] Qing-Hong Cao, Ernest Ma, and G. Rajasekaran. “Observing the Dark Scalar Doublet and its Impact on the Standard-Model Higgs Boson at Colliders”. In: *Phys. Rev. D* 76 (2007), p. 095011. DOI: [10.1103/PhysRevD.76.095011](https://doi.org/10.1103/PhysRevD.76.095011). arXiv: [0708.2939](https://arxiv.org/abs/0708.2939) [[hep-ph](#)].
- [11] Prateek Agrawal, Ethan M. Dolle, and Christopher A. Krenke. “Signals of Inert Doublet Dark Matter in Neutrino Telescopes”. In: *Phys. Rev. D* 79 (2009), p. 015015. DOI: [10.1103/PhysRevD.79.015015](https://doi.org/10.1103/PhysRevD.79.015015). arXiv: [0811.1798](https://arxiv.org/abs/0811.1798) [[hep-ph](#)].
- [12] Erik Lundstrom, Michael Gustafsson, and Joakim Edsjo. “The Inert Doublet Model and LEP II Limits”. In: *Phys. Rev. D* 79 (2009), p. 035013. DOI: [10.1103/PhysRevD.79.035013](https://doi.org/10.1103/PhysRevD.79.035013). arXiv: [0810.3924](https://arxiv.org/abs/0810.3924) [[hep-ph](#)].
- [13] T. Hambye et al. “Scalar Multiplet Dark Matter”. In: *JHEP* 07 (2009). [Erratum: *JHEP*05,066(2010)], p. 090. DOI: [10.1007/JHEP05\(2010\)066](https://doi.org/10.1007/JHEP05(2010)066), [10.1088/1126-6708/2009/07/090](https://doi.org/10.1088/1126-6708/2009/07/090). arXiv: [0903.4010](https://arxiv.org/abs/0903.4010) [[hep-ph](#)].
- [14] Sarah Andreas, Michel H. G. Tytgat, and Quentin Swillens. “Neutrinos from Inert Doublet Dark Matter”. In: *JCAP* 0904 (2009), p. 004. DOI: [10.1088/1475-7516/2009/04/004](https://doi.org/10.1088/1475-7516/2009/04/004). arXiv: [0901.1750](https://arxiv.org/abs/0901.1750) [[hep-ph](#)].
- [15] Emmanuel Nezri, Michel H. G. Tytgat, and Gilles Vertongen. “e⁺ and anti-p from inert doublet model dark matter”. In: *JCAP* 0904 (2009), p. 014. DOI: [10.1088/1475-7516/2009/04/014](https://doi.org/10.1088/1475-7516/2009/04/014). arXiv: [0901.2556](https://arxiv.org/abs/0901.2556) [[hep-ph](#)].
- [16] Chiara Arina, Fu-Sin Ling, and Michel H. G. Tytgat. “IDM and iDM or The Inert Doublet Model and Inelastic Dark Matter”. In: *JCAP* 0910 (2009), p. 018. DOI: [10.1088/1475-7516/2009/10/018](https://doi.org/10.1088/1475-7516/2009/10/018). arXiv: [0907.0430](https://arxiv.org/abs/0907.0430) [[hep-ph](#)].
- [17] Ethan Dolle et al. “Dilepton Signals in the Inert Doublet Model”. In: *Phys. Rev. D* 81 (2010), p. 035003. DOI: [10.1103/PhysRevD.81.035003](https://doi.org/10.1103/PhysRevD.81.035003). arXiv: [0909.3094](https://arxiv.org/abs/0909.3094) [[hep-ph](#)].
- [18] Laura Lopez Honorez and Carlos E. Yaguna. “A new viable region of the inert doublet model”. In: *JCAP* 1101 (2011), p. 002. DOI: [10.1088/1475-7516/2011/01/002](https://doi.org/10.1088/1475-7516/2011/01/002). arXiv: [1011.1411](https://arxiv.org/abs/1011.1411) [[hep-ph](#)].
- [19] Laura Lopez Honorez and Carlos E. Yaguna. “The inert doublet model of dark matter revisited”. In: *JHEP* 09 (2010), p. 046. DOI: [10.1007/JHEP09\(2010\)046](https://doi.org/10.1007/JHEP09(2010)046). arXiv: [1003.3125](https://arxiv.org/abs/1003.3125) [[hep-ph](#)].
- [20] I. F. Ginzburg et al. “Evolution of Universe to the present inert phase”. In: *Phys. Rev. D* 82 (2010), p. 123533. DOI: [10.1103/PhysRevD.82.123533](https://doi.org/10.1103/PhysRevD.82.123533). arXiv: [1009.4593](https://arxiv.org/abs/1009.4593) [[hep-ph](#)].

- [21] M. Hirsch et al. “Discrete dark matter”. In: *Phys. Rev. D* 82 (2010), p. 116003. DOI: [10.1103/PhysRevD.82.116003](https://doi.org/10.1103/PhysRevD.82.116003). arXiv: [1007.0871](https://arxiv.org/abs/1007.0871) [hep-ph].
- [22] Xinyu Miao, Shufang Su, and Brooks Thomas. “Trilepton Signals in the Inert Doublet Model”. In: *Phys. Rev. D* 82 (2010), p. 035009. DOI: [10.1103/PhysRevD.82.035009](https://doi.org/10.1103/PhysRevD.82.035009). arXiv: [1005.0090](https://arxiv.org/abs/1005.0090) [hep-ph].
- [23] Abdesslam Arhrib, Rachid Benbrik, and Naveen Gaur. “ $H \rightarrow \gamma\gamma$ in Inert Higgs Doublet Model”. In: *Phys. Rev. D* 85 (2012), p. 095021. DOI: [10.1103/PhysRevD.85.095021](https://doi.org/10.1103/PhysRevD.85.095021). arXiv: [1201.2644](https://arxiv.org/abs/1201.2644) [hep-ph].
- [24] Bogumila Swiezewska and Maria Krawczyk. “Diphoton rate in the inert doublet model with a 125 GeV Higgs boson”. In: *Phys. Rev. D* 88.3 (2013), p. 035019. DOI: [10.1103/PhysRevD.88.035019](https://doi.org/10.1103/PhysRevD.88.035019). arXiv: [1212.4100](https://arxiv.org/abs/1212.4100) [hep-ph].
- [25] Michael Klasen, Carlos E. Yaguna, and Jose D. Ruiz-Alvarez. “Electroweak corrections to the direct detection cross section of inert higgs dark matter”. In: *Phys. Rev. D* 87 (2013), p. 075025. DOI: [10.1103/PhysRevD.87.075025](https://doi.org/10.1103/PhysRevD.87.075025). arXiv: [1302.1657](https://arxiv.org/abs/1302.1657) [hep-ph].
- [26] Camilo Garcia-Cely and Alejandro Ibarra. “Novel Gamma-ray Spectral Features in the Inert Doublet Model”. In: *JCAP* 1309 (2013), p. 025. DOI: [10.1088/1475-7516/2013/09/025](https://doi.org/10.1088/1475-7516/2013/09/025). arXiv: [1306.4681](https://arxiv.org/abs/1306.4681) [hep-ph].
- [27] Maria Krawczyk et al. “Constraining Inert Dark Matter by $R_{\gamma\gamma}$ and WMAP data”. In: *JHEP* 09 (2013), p. 055. DOI: [10.1007/JHEP09\(2013\)055](https://doi.org/10.1007/JHEP09(2013)055). arXiv: [1305.6266](https://arxiv.org/abs/1305.6266) [hep-ph].
- [28] A. Goudelis, B. Herrmann, and O. Stål. “Dark matter in the Inert Doublet Model after the discovery of a Higgs-like boson at the LHC”. In: *JHEP* 09 (2013), p. 106. DOI: [10.1007/JHEP09\(2013\)106](https://doi.org/10.1007/JHEP09(2013)106). arXiv: [1303.3010](https://arxiv.org/abs/1303.3010) [hep-ph].
- [29] Camilo Garcia-Cely, Michael Gustafsson, and Alejandro Ibarra. “Probing the Inert Doublet Dark Matter Model with Cherenkov Telescopes”. In: *JCAP* 1602.02 (2016), p. 043. DOI: [10.1088/1475-7516/2016/02/043](https://doi.org/10.1088/1475-7516/2016/02/043). arXiv: [1512.02801](https://arxiv.org/abs/1512.02801) [hep-ph].
- [30] Farinaldo S. Queiroz and Carlos E. Yaguna. “The CTA aims at the Inert Doublet Model”. In: *JCAP* 1602.02 (2016), p. 038. DOI: [10.1088/1475-7516/2016/02/038](https://doi.org/10.1088/1475-7516/2016/02/038). arXiv: [1511.05967](https://arxiv.org/abs/1511.05967) [hep-ph].
- [31] Alexander Belyaev et al. “Anatomy of the Inert Two Higgs Doublet Model in the light of the LHC and non-LHC Dark Matter Searches”. In: *Phys. Rev. D* 97.3 (2018), p. 035011. DOI: [10.1103/PhysRevD.97.035011](https://doi.org/10.1103/PhysRevD.97.035011). arXiv: [1612.00511](https://arxiv.org/abs/1612.00511) [hep-ph].
- [32] Benedikt Eiteneuer, Andreas Goudelis, and Jan Heisig. “The inert doublet model in the light of Fermi-LAT gamma-ray data: a global fit analysis”. In: *Eur. Phys. J. C* 77.9 (2017), p. 624. DOI: [10.1140/epjc/s10052-017-5166-1](https://doi.org/10.1140/epjc/s10052-017-5166-1). arXiv: [1705.01458](https://arxiv.org/abs/1705.01458) [hep-ph].
- [33] S. Biondini and M. Laine. “Re-derived overclosure bound for the inert doublet model”. In: *JHEP* 08 (2017), p. 047. DOI: [10.1007/JHEP08\(2017\)047](https://doi.org/10.1007/JHEP08(2017)047). arXiv: [1706.01894](https://arxiv.org/abs/1706.01894) [hep-ph].
- [34] Bhaskar Dutta et al. “Vector Boson Fusion in the Inert Doublet Model”. In: *Phys. Rev. D* 97.5 (2018), p. 055045. DOI: [10.1103/PhysRevD.97.055045](https://doi.org/10.1103/PhysRevD.97.055045). arXiv: [1709.09796](https://arxiv.org/abs/1709.09796) [hep-ph].
- [35] Neng Wan et al. “Searches for Dark Matter via Mono-W Production in Inert Doublet Model at the LHC”. In: *Commun. Theor. Phys.* 69.5 (2018), p. 617. DOI: [10.1088/0253-6102/69/5/617](https://doi.org/10.1088/0253-6102/69/5/617).

- [36] A. Belyaev et al. “Advancing LHC probes of dark matter from the inert two-Higgs-doublet model with the monojet signal”. In: *Phys. Rev. D* 99.1 (2019), p. 015011. DOI: [10.1103/PhysRevD.99.015011](https://doi.org/10.1103/PhysRevD.99.015011). arXiv: [1809.00933](https://arxiv.org/abs/1809.00933) [hep-ph].
- [37] Jan Kalinowski et al. “Exploring Inert Scalars at CLIC”. In: *JHEP* 07 (2019), p. 053. DOI: [10.1007/JHEP07\(2019\)053](https://doi.org/10.1007/JHEP07(2019)053). arXiv: [1811.06952](https://arxiv.org/abs/1811.06952) [hep-ph].
- [38] Sandip Pakvasa and Hirotaka Sugawara. “Discrete Symmetry and Cabibbo Angle”. In: *Phys. Lett.* B73 (1978), pp. 61–64. DOI: [10.1016/0370-2693\(78\)90172-7](https://doi.org/10.1016/0370-2693(78)90172-7).
- [39] Emanuel Derman. “Flavor Unification, τ Decay and b Decay Within the Six Quark Six Lepton Weinberg-Salam Model”. In: *Phys. Rev. D* 19 (1979), pp. 317–329. DOI: [10.1103/PhysRevD.19.317](https://doi.org/10.1103/PhysRevD.19.317).
- [40] Emanuel Derman and Hung-Sheng Tsao. “SU(2) X U(1) X S(n) Flavor Dynamics and a Bound on the Number of Flavors”. In: *Phys. Rev. D* 20 (1979), p. 1207. DOI: [10.1103/PhysRevD.20.1207](https://doi.org/10.1103/PhysRevD.20.1207).
- [41] A. Mondragon and E. Rodriguez-Jauregui. “Breaking of flavor permutational symmetry and the CKM matrix”. In: *AIP Conf. Proc.* 531 (2000). [AIP Conf. Proc.490,393(1999)], pp. 310–314. DOI: [10.1063/1.1315055](https://doi.org/10.1063/1.1315055).
- [42] J. Kubo et al. “The Flavor symmetry”. In: *Prog. Theor. Phys.* 109 (2003). [Erratum: Prog. Theor. Phys.114,287(2005)], pp. 795–807. DOI: [10.1143/PTP.109.795](https://doi.org/10.1143/PTP.109.795). arXiv: [hep-ph/0302196](https://arxiv.org/abs/hep-ph/0302196) [hep-ph].
- [43] Jisuke Kubo, Hiroshi Okada, and Fumiaki Sakamaki. “Higgs potential in minimal S(3) invariant extension of the standard model”. In: *Phys. Rev. D* 70 (2004), p. 036007. DOI: [10.1103/PhysRevD.70.036007](https://doi.org/10.1103/PhysRevD.70.036007). arXiv: [hep-ph/0402089](https://arxiv.org/abs/hep-ph/0402089) [hep-ph].
- [44] A. Mondragon, M. Mondragon, and E. Peinado. “Lepton masses, mixings and FCNC in a minimal S(3)-invariant extension of the Standard Model”. In: *Phys. Rev. D* 76 (2007), p. 076003. DOI: [10.1103/PhysRevD.76.076003](https://doi.org/10.1103/PhysRevD.76.076003). arXiv: [0706.0354](https://arxiv.org/abs/0706.0354) [hep-ph].
- [45] F. Gonzalez Canales, A. Mondragon, and M. Mondragon. “The S_3 Flavour Symmetry: Neutrino Masses and Mixings”. In: *Fortsch. Phys.* 61 (2013), pp. 546–570. DOI: [10.1002/prop.201200121](https://doi.org/10.1002/prop.201200121). arXiv: [1205.4755](https://arxiv.org/abs/1205.4755) [hep-ph].
- [46] Tadayuki Teshima. “Higgs potential in S_3 invariant model for quark-lepton mass and mixing”. In: *Phys. Rev. D* 85 (2012), p. 105013. DOI: [10.1103/PhysRevD.85.105013](https://doi.org/10.1103/PhysRevD.85.105013). arXiv: [1202.4528](https://arxiv.org/abs/1202.4528) [hep-ph].
- [47] F. González Canales et al. “Quark sector of S3 models: classification and comparison with experimental data”. In: *Phys. Rev. D* 88 (2013), p. 096004. DOI: [10.1103/PhysRevD.88.096004](https://doi.org/10.1103/PhysRevD.88.096004). arXiv: [1304.6644](https://arxiv.org/abs/1304.6644) [hep-ph].
- [48] Dipankar Das and Ujjal Kumar Dey. “Analysis of an extended scalar sector with S_3 symmetry”. In: *Phys. Rev. D* 89.9 (2014). [Erratum: Phys. Rev.D91,no.3,039905(2015)], p. 095025. DOI: [10.1103/PhysRevD.91.039905](https://doi.org/10.1103/PhysRevD.91.039905), [10.1103/PhysRevD.89.095025](https://doi.org/10.1103/PhysRevD.89.095025). arXiv: [1404.2491](https://arxiv.org/abs/1404.2491) [hep-ph].
- [49] E. Barradas-Guevara, O. Félix-Beltrán, and E. Rodriguez-Jáuregui. “Trilinear self-couplings in an S(3) flavored Higgs model”. In: *Phys. Rev. D* 90.9 (2014), p. 095001. DOI: [10.1103/PhysRevD.90.095001](https://doi.org/10.1103/PhysRevD.90.095001). arXiv: [1402.2244](https://arxiv.org/abs/1402.2244) [hep-ph].

- [50] D. Emmanuel-Costa et al. “Spontaneous symmetry breaking in the S_3 -symmetric scalar sector”. In: *JHEP* 02 (2016), p. 154. DOI: [10.1007/JHEP02\(2016\)154](https://doi.org/10.1007/JHEP02(2016)154). arXiv: [1601.04654](https://arxiv.org/abs/1601.04654) [hep-ph].
- [51] Dipankar Das, Ujjal Kumar Dey, and Palash B. Pal. “ S_3 symmetry and the quark mixing matrix”. In: *Phys. Lett.* B753 (2016), pp. 315–318. DOI: [10.1016/j.physletb.2015.12.038](https://doi.org/10.1016/j.physletb.2015.12.038). arXiv: [1507.06509](https://arxiv.org/abs/1507.06509) [hep-ph].
- [52] E. Barradas-Guevara, O. Félix-Beltrán, and E. Rodríguez-Jáuregui. “CP breaking in $S(3)$ flavoured Higgs model”. In: (2015). arXiv: [1507.05180](https://arxiv.org/abs/1507.05180) [hep-ph].
- [53] C. Espinoza et al. “The S_3 Symmetric Model with a Dark Scalar”. In: *Phys. Lett.* B788 (2019), pp. 185–191. DOI: [10.1016/j.physletb.2018.11.028](https://doi.org/10.1016/j.physletb.2018.11.028). arXiv: [1804.01879](https://arxiv.org/abs/1804.01879) [hep-ph].
- [54] Juan Carlos Gómez-Izquierdo and Myriam Mondragón. “B–L Model with S_3 symmetry: Nearest Neighbor Interaction Textures and Broken $\mu \leftrightarrow \tau$ Symmetry”. In: *Eur. Phys. J.* C79.3 (2019), p. 285. DOI: [10.1140/epjc/s10052-019-6785-5](https://doi.org/10.1140/epjc/s10052-019-6785-5). arXiv: [1804.08746](https://arxiv.org/abs/1804.08746) [hep-ph].
- [55] E. A. Garcés, Juan Carlos Gómez-Izquierdo, and F. Gonzalez-Canales. “Flavored non-minimal left–right symmetric model fermion masses and mixings”. In: *Eur. Phys. J.* C78.10 (2018), p. 812. DOI: [10.1140/epjc/s10052-018-6271-5](https://doi.org/10.1140/epjc/s10052-018-6271-5). arXiv: [1807.02727](https://arxiv.org/abs/1807.02727) [hep-ph].
- [56] Subhasmita Mishra. “Majorana dark matter and neutrino mass with S_3 symmetry”. In: (2019). arXiv: [1911.02255](https://arxiv.org/abs/1911.02255) [hep-ph].
- [57] Nabarun Chakrabarty and Indrani Chakraborty. “Flavour-alignment in an S_3 -symmetric Higgs sector and its RG-behaviour”. In: (2019). arXiv: [1903.09388](https://arxiv.org/abs/1903.09388) [hep-ph].
- [58] A. Kuncinas et al. “A class of S_3 -inspired Three-Higgs-Doublet Models with complex vacuum”. In: (2020). arXiv: [2001.01994](https://arxiv.org/abs/2001.01994) [hep-ph].
- [59] A. E. Cárcamo Hernández et al. “Fermion spectrum and $g - 2$ anomalies in a low scale 3-3-1 model”. In: (2020). arXiv: [2002.07347](https://arxiv.org/abs/2002.07347) [hep-ph].
- [60] Junji Hisano, S. Matsumoto, and Mihoko M. Nojiri. “Unitarity and higher order corrections in neutralino dark matter annihilation into two photons”. In: *Phys. Rev.* D67 (2003), p. 075014. DOI: [10.1103/PhysRevD.67.075014](https://doi.org/10.1103/PhysRevD.67.075014). arXiv: [hep-ph/0212022](https://arxiv.org/abs/hep-ph/0212022) [hep-ph].
- [61] Junji Hisano et al. “Non-perturbative effect on dark matter annihilation and gamma ray signature from galactic center”. In: *Phys. Rev.* D71 (2005), p. 063528. DOI: [10.1103/PhysRevD.71.063528](https://doi.org/10.1103/PhysRevD.71.063528). arXiv: [hep-ph/0412403](https://arxiv.org/abs/hep-ph/0412403) [hep-ph].
- [62] Junji Hisano, Shigeki Matsumoto, and Mihoko M. Nojiri. “Explosive dark matter annihilation”. In: *Phys. Rev. Lett.* 92 (2004), p. 031303. DOI: [10.1103/PhysRevLett.92.031303](https://doi.org/10.1103/PhysRevLett.92.031303). arXiv: [hep-ph/0307216](https://arxiv.org/abs/hep-ph/0307216) [hep-ph].
- [63] M. Beneke, C. Hellmann, and P. Ruiz-Femenia. “Non-relativistic pair annihilation of nearly mass degenerate neutralinos and charginos III. Computation of the Sommerfeld enhancements”. In: *JHEP* 05 (2015), p. 115. DOI: [10.1007/JHEP05\(2015\)115](https://doi.org/10.1007/JHEP05(2015)115). arXiv: [1411.6924](https://arxiv.org/abs/1411.6924) [hep-ph].
- [64] Camilo Garcia-Cely et al. “Gamma-rays from Heavy Minimal Dark Matter”. In: *JCAP* 1510.10 (2015), p. 058. DOI: [10.1088/1475-7516/2015/10/058](https://doi.org/10.1088/1475-7516/2015/10/058). arXiv: [1507.05536](https://arxiv.org/abs/1507.05536) [hep-ph].

- [65] Lars Bergstrom, Piero Ullio, and James H. Buckley. “Observability of gamma-rays from dark matter neutralino annihilations in the Milky Way halo”. In: *Astropart. Phys.* 9 (1998), pp. 137–162. DOI: [10.1016/S0927-6505\(98\)00015-2](https://doi.org/10.1016/S0927-6505(98)00015-2). arXiv: [astro-ph/9712318](https://arxiv.org/abs/astro-ph/9712318) [[astro-ph](#)].
- [66] Alex Geringer-Sameth, Savvas M. Koushiappas, and Matthew Walker. “Dwarf galaxy annihilation and decay emission profiles for dark matter experiments”. In: *Astrophys. J.* 801.2 (2015), p. 74. DOI: [10.1088/0004-637X/801/2/74](https://doi.org/10.1088/0004-637X/801/2/74). arXiv: [1408.0002](https://arxiv.org/abs/1408.0002) [[astro-ph.CO](#)].
- [67] V. Belokurov et al. “Cats and Dogs, Hair and A Hero: A Quintet of New Milky Way Companions”. In: *Astrophys. J.* 654 (2007), pp. 897–906. DOI: [10.1086/509718](https://doi.org/10.1086/509718). arXiv: [astro-ph/0608448](https://arxiv.org/abs/astro-ph/0608448) [[astro-ph](#)].
- [68] H. Abdalla et al. “Searches for gamma-ray lines and ‘pure WIMP’ spectra from Dark Matter annihilations in dwarf galaxies with H.E.S.S”. In: *JCAP* 1811.11 (2018), p. 037. DOI: [10.1088/1475-7516/2018/11/037](https://doi.org/10.1088/1475-7516/2018/11/037). arXiv: [1810.00995](https://arxiv.org/abs/1810.00995) [[astro-ph.HE](#)].
- [69] F. Aharonian et al. “Observations of the Crab Nebula with H.E.S.S”. In: *Astron. Astrophys.* 457 (2006), pp. 899–915. DOI: [10.1051/0004-6361:20065351](https://doi.org/10.1051/0004-6361:20065351). arXiv: [astro-ph/0607333](https://arxiv.org/abs/astro-ph/0607333) [[astro-ph](#)].
- [70] Gregory D. Martinez et al. “Comparison of statistical sampling methods with ScannerBit, the GAMBIT scanning module”. In: *Eur. Phys. J.* C77.11 (2017), p. 761. DOI: [10.1140/epjc/s10052-017-5274-y](https://doi.org/10.1140/epjc/s10052-017-5274-y). arXiv: [1705.07959](https://arxiv.org/abs/1705.07959) [[hep-ph](#)].
- [71] Peter Athron et al. “GAMBIT: The Global and Modular Beyond-the-Standard-Model Inference Tool”. In: *Eur. Phys. J.* C77.11 (2017). [Addendum: *Eur. Phys. J.* C78,no.2,98(2018)], p. 784. DOI: [10.1140/epjc/s10052-017-5513-2](https://doi.org/10.1140/epjc/s10052-017-5513-2), [10.1140/epjc/s10052-017-5321-8](https://doi.org/10.1140/epjc/s10052-017-5321-8). arXiv: [1705.07908](https://arxiv.org/abs/1705.07908) [[hep-ph](#)].
- [72] Pat Scott. “Pippi - painless parsing, post-processing and plotting of posterior and likelihood samples”. In: *Eur. Phys. J. Plus* 127 (2012), p. 138. DOI: [10.1140/epjp/i2012-12138-3](https://doi.org/10.1140/epjp/i2012-12138-3). arXiv: [1206.2245](https://arxiv.org/abs/1206.2245) [[physics.data-an](#)].
- [73] Georges Aad et al. “Observation of a new particle in the search for the Standard Model Higgs boson with the ATLAS detector at the LHC”. In: *Phys. Lett.* B716 (2012), pp. 1–29. DOI: [10.1016/j.physletb.2012.08.020](https://doi.org/10.1016/j.physletb.2012.08.020). arXiv: [1207.7214](https://arxiv.org/abs/1207.7214) [[hep-ex](#)].
- [74] Serguei Chatrchyan et al. “Observation of a new boson at a mass of 125 GeV with the CMS experiment at the LHC”. In: *Phys. Lett.* B716 (2012), pp. 30–61. DOI: [10.1016/j.physletb.2012.08.021](https://doi.org/10.1016/j.physletb.2012.08.021). arXiv: [1207.7235](https://arxiv.org/abs/1207.7235) [[hep-ex](#)].
- [75] Florian Staub. “SARAH 4 : A tool for (not only SUSY) model builders”. In: *Comput. Phys. Commun.* 185 (2014), pp. 1773–1790. DOI: [10.1016/j.cpc.2014.02.018](https://doi.org/10.1016/j.cpc.2014.02.018). arXiv: [1309.7223](https://arxiv.org/abs/1309.7223) [[hep-ph](#)].
- [76] Florian Staub. “From Superpotential to Model Files for FeynArts and CalcHep/CompHep”. In: *Comput. Phys. Commun.* 181 (2010), pp. 1077–1086. DOI: [10.1016/j.cpc.2010.01.011](https://doi.org/10.1016/j.cpc.2010.01.011). arXiv: [0909.2863](https://arxiv.org/abs/0909.2863) [[hep-ph](#)].
- [77] Florian Staub. “Automatic Calculation of supersymmetric Renormalization Group Equations and Self Energies”. In: *Comput. Phys. Commun.* 182 (2011), pp. 808–833. DOI: [10.1016/j.cpc.2010.11.030](https://doi.org/10.1016/j.cpc.2010.11.030). arXiv: [1002.0840](https://arxiv.org/abs/1002.0840) [[hep-ph](#)].
- [78] Florian Staub. “SARAH 3.2: Dirac Gauginos, UFO output, and more”. In: *Comput. Phys. Commun.* 184 (2013), pp. 1792–1809. DOI: [10.1016/j.cpc.2013.02.019](https://doi.org/10.1016/j.cpc.2013.02.019). arXiv: [1207.0906](https://arxiv.org/abs/1207.0906) [[hep-ph](#)].

- [79] Benjamin W. Lee, C. Quigg, and H. B. Thacker. “Weak Interactions at Very High-Energies: The Role of the Higgs Boson Mass”. In: *Phys. Rev. D* 16 (1977), p. 1519. DOI: [10.1103/PhysRevD.16.1519](https://doi.org/10.1103/PhysRevD.16.1519).
- [80] Mark D. Goodsell and Florian Staub. “Unitarity constraints on general scalar couplings with SARAH”. In: *Eur. Phys. J. C* 78.8 (2018), p. 649. DOI: [10.1140/epjc/s10052-018-6127-z](https://doi.org/10.1140/epjc/s10052-018-6127-z). arXiv: [1805.07306 \[hep-ph\]](https://arxiv.org/abs/1805.07306).
- [81] Florian Staub. “Exploring new models in all detail with SARAH”. In: *Adv. High Energy Phys.* 2015 (2015), p. 840780. DOI: [10.1155/2015/840780](https://doi.org/10.1155/2015/840780). arXiv: [1503.04200 \[hep-ph\]](https://arxiv.org/abs/1503.04200).
- [82] Werner Porod. “SPHeno, a program for calculating supersymmetric spectra, SUSY particle decays and SUSY particle production at e^+e^- colliders”. In: *Comput. Phys. Commun.* 153 (2003), pp. 275–315. DOI: [10.1016/S0010-4655\(03\)00222-4](https://doi.org/10.1016/S0010-4655(03)00222-4). arXiv: [hep-ph/0301101 \[hep-ph\]](https://arxiv.org/abs/hep-ph/0301101).
- [83] W. Porod and F. Staub. “SPHeno 3.1: Extensions including flavour, CP-phases and models beyond the MSSM”. In: *Comput. Phys. Commun.* 183 (2012), pp. 2458–2469. DOI: [10.1016/j.cpc.2012.05.021](https://doi.org/10.1016/j.cpc.2012.05.021). arXiv: [1104.1573 \[hep-ph\]](https://arxiv.org/abs/1104.1573).
- [84] Philip Bechtle et al. “HiggsBounds: Confronting Arbitrary Higgs Sectors with Exclusion Bounds from LEP and the Tevatron”. In: *Comput. Phys. Commun.* 181 (2010), pp. 138–167. DOI: [10.1016/j.cpc.2009.09.003](https://doi.org/10.1016/j.cpc.2009.09.003). arXiv: [0811.4169 \[hep-ph\]](https://arxiv.org/abs/0811.4169).
- [85] Philip Bechtle et al. “HiggsBounds 2.0.0: Confronting Neutral and Charged Higgs Sector Predictions with Exclusion Bounds from LEP and the Tevatron”. In: *Comput. Phys. Commun.* 182 (2011), pp. 2605–2631. DOI: [10.1016/j.cpc.2011.07.015](https://doi.org/10.1016/j.cpc.2011.07.015). arXiv: [1102.1898 \[hep-ph\]](https://arxiv.org/abs/1102.1898).
- [86] Philip Bechtle et al. “Recent Developments in HiggsBounds and a Preview of HiggsSignals”. In: *PoS CHARGED2012* (2012), p. 024. arXiv: [1301.2345 \[hep-ph\]](https://arxiv.org/abs/1301.2345).
- [87] Philip Bechtle et al. “HiggsBounds-4: Improved Tests of Extended Higgs Sectors against Exclusion Bounds from LEP, the Tevatron and the LHC”. In: *Eur. Phys. J. C* 74 (2014), p. 2693. arXiv: [1311.0055 \[hep-ph\]](https://arxiv.org/abs/1311.0055).
- [88] Philip Bechtle et al. “Applying Exclusion Likelihoods from LHC Searches to Extended Higgs Sectors”. In: (2015). arXiv: [1507.06706 \[hep-ph\]](https://arxiv.org/abs/1507.06706).
- [89] William H. Press et al. *Numerical Recipes in C (2nd Ed.): The Art of Scientific Computing*. USA: Cambridge University Press, 1992. ISBN: 0521431085.
- [90] Thomas Hahn. “Generating Feynman diagrams and amplitudes with FeynArts 3”. In: *Comput. Phys. Commun.* 140 (2001), pp. 418–431. DOI: [10.1016/S0010-4655\(01\)00290-9](https://doi.org/10.1016/S0010-4655(01)00290-9). arXiv: [hep-ph/0012260 \[hep-ph\]](https://arxiv.org/abs/hep-ph/0012260).
- [91] T. Hahn and M. Perez-Victoria. “Automatized one loop calculations in four-dimensions and D-dimensions”. In: *Comput. Phys. Commun.* 118 (1999), pp. 153–165. DOI: [10.1016/S0010-4655\(98\)00173-8](https://doi.org/10.1016/S0010-4655(98)00173-8). arXiv: [hep-ph/9807565 \[hep-ph\]](https://arxiv.org/abs/hep-ph/9807565).
- [92] R. Mertig, M. Bohm, and Ansgar Denner. “FEYN CALC: Computer algebraic calculation of Feynman amplitudes”. In: *Comput. Phys. Commun.* 64 (1991), pp. 345–359. DOI: [10.1016/0010-4655\(91\)90130-D](https://doi.org/10.1016/0010-4655(91)90130-D).
- [93] Vladyslav Shtabovenko, Rolf Mertig, and Frederik Orellana. “New Developments in FeynCalc 9.0”. In: *Comput. Phys. Commun.* 207 (2016), pp. 432–444. DOI: [10.1016/j.cpc.2016.06.008](https://doi.org/10.1016/j.cpc.2016.06.008). arXiv: [1601.01167 \[hep-ph\]](https://arxiv.org/abs/1601.01167).

- [94] Vladyslav Shtabovenko, Rolf Mertig, and Frederik Orellana. “FeynCalc 9.3: New features and improvements”. In: (2020). arXiv: [2001.04407](https://arxiv.org/abs/2001.04407) [[hep-ph](#)].
- [95] J. Knödlseeder et al. “GammaLib and ctools: A software framework for the analysis of astronomical gamma-ray data”. In: *Astron. Astrophys.* 593 (2016), A1. DOI: [10.1051/0004-6361/201628822](https://doi.org/10.1051/0004-6361/201628822). arXiv: [1606.00393](https://arxiv.org/abs/1606.00393) [[astro-ph.IM](#)].
- [96] CTA Consortium. *CTA Scientific Analysis Software*. <http://ascl.net/1601.005> and <http://ascl.net/1110.007>. 2020. URL: <http://cta.irap.omp.eu/ctools/>.
- [97] D. Barducci et al. “Collider limits on new physics within micrOMEGAs 4.3”. In: *Comput. Phys. Commun.* 222 (2018), pp. 327–338. DOI: [10.1016/j.cpc.2017.08.028](https://doi.org/10.1016/j.cpc.2017.08.028). arXiv: [1606.03834](https://arxiv.org/abs/1606.03834) [[hep-ph](#)].
- [98] N. Aghanim et al. “Planck 2018 results. VI. Cosmological parameters”. In: (2018). arXiv: [1807.06209](https://arxiv.org/abs/1807.06209) [[astro-ph.CO](#)].
- [99] URL: <https://gitlab.com/catalina.ehdz/heavyS3>.
- [100] Valentin Lefranc, Gary A. Mamon, and Paolo Panci. “Prospects for annihilating Dark Matter towards Milky Way’s dwarf galaxies by the Cherenkov Telescope Array”. In: *JCAP* 09 (2016), p. 021. DOI: [10.1088/1475-7516/2016/09/021](https://doi.org/10.1088/1475-7516/2016/09/021). arXiv: [1605.02793](https://arxiv.org/abs/1605.02793) [[astro-ph.HE](#)].
- [101] M. Tanabashi et al. “Review of Particle Physics”. In: *Phys. Rev. D* 98.3 (2018), p. 030001. DOI: [10.1103/PhysRevD.98.030001](https://doi.org/10.1103/PhysRevD.98.030001).
- [102] CTA Consortium. *CTA’s expected baseline performance*. 2020. URL: <https://www.cta-observatory.org/science/cta-performance/>.
- [103] W. A. Joye and E. Mandel. “New Features of SAOImage DS9”. In: *Astronomical Data Analysis Software and Systems XII*. Ed. by H. E. Payne, R. I. Jedrzejewski, and R. N. Hook. Vol. 295. Astronomical Society of the Pacific Conference Series. Jan. 2003, p. 489.